

2XMM Ultraluminous X-Ray Source Candidates in Nearby Galaxies

D. J. Walton¹ ^{*}, T. P. Roberts² [†], S. Mateos³ & V. Heard³

¹ *Institute of Astronomy, Cambridge University, Madingley Road, Cambridge, CB3 0HA*

² *Department of Physics, Durham University, South Road, Durham DH1 3LE, UK*

³ *Department of Physics and Astronomy, University of Leicester, University Road, Leicester, UK*

ABSTRACT

Ultraluminous X-ray sources (ULXs) are some of the most enigmatic X-ray bright sources known to date. It is generally accepted that they cannot host black holes as large as those associated with active galaxies, but they appear to be significantly more luminous than their better understood Galactic X-ray binary (XRB) cousins, while displaying an intriguing combination of differences and similarities with them. Through studying large, representative samples of these sources we may hope to enhance our understanding of them. To this end, we derive a large catalogue of 650 X-ray detections of 470 ULX candidates, located in 238 nearby galaxies, by cross correlating the 2XMM Serendipitous Survey with the Third Reference Catalogue of Bright Galaxies. The presented dedicated catalogue offers a significant improvement over those previously published both in terms of number and the contribution of background contaminants, *e.g.* distant quasars, which we estimate to be at most 24 per cent, but more likely ~ 17 per cent. To undertake population studies, we define a ‘complete’ sub-sample of sources compiled from observations of galaxies with sensitivity limits below 10^{39} erg s⁻¹. The luminosity function of this sample is consistent with a simple power-law of form $N(> L_X) \propto L_X^{-0.96 \pm 0.11}$. Although we do not find any statistical requirement for a cut-off luminosity of $L_c \sim 10^{40}$ erg s⁻¹, as has been reported previously, we are not able to rule out its presence. Also, we find that the number of ULXs per unit galaxy mass, S^u decreases with increasing galaxy mass for ULXs associated with spiral galaxies, and is well modelled with a power-law of form $S^u \propto M^{-0.64 \pm 0.07}$. This is in broad agreement with previous results, and is likely to be a consequence of the decrease in specific star formation and increase in metallicity with increasing spiral galaxy mass. S^u is consistent with being constant with galaxy mass for sources associated with elliptical galaxies, implying this older ULX population traces stellar mass rather than star formation.

Key words: X-rays: binaries – black hole physics

1 INTRODUCTION

The first X-ray imaging observations of galaxies beyond the local group, obtained with the *Einstein* observatory in the early 1980s, lead to the discovery of a new population of extremely bright, extra-nuclear X-ray sources with luminosities $L_X > 10^{39}$ erg s⁻¹ (Fabbiano 1989). Such sources are now commonly referred to as ultraluminous X-ray sources (ULXs), and remain the subject of continuing speculation as to how they are able to radiate so brightly. The observed luminosities imply some kind of accreting black hole, but they are (or at least appear) brighter than the traditional Eddington limit for the ‘stellar mass’ black holes in X-ray binaries (BHBs) observed in our own galaxy ($M_{\text{BH}} \sim 10 M_\odot$). However, it is generally accepted that these are not extra-nuclear examples of the supermassive black holes (SMBH; $M_{\text{BH}} > 10^{5-6} M_\odot$) expected to power active galactic nuclei, as such objects should sink to their

galaxy centres comfortably within a Hubble time due to dynamical friction (Miller & Colbert 2004).

Improvements in the available X-ray instrumentation, especially with the launch of the *XMM-Newton* and *Chandra* observatories, combined with multi-wavelength studies have improved our understanding of ULXs considerably in recent years, but the exact cause of the apparently extreme luminosities has yet to be determined unambiguously for any individual source, let alone for the population as a whole. Most of the proposed explanations revolve around one of the three following ideas. The first is that the black holes powering ULXs are simply much more massive than those in BHBs (see *e.g.* Colbert & Mushotzky 1999), perhaps the long sought after intermediate-mass black holes (IMBHs; $10^2 M_\odot \lesssim M_{\text{BH}} \lesssim 10^4 M_\odot$), accreting at rates substantially below the Eddington limit as per Galactic BHBs. The second is that the black holes hosted by ULXs are essentially the same as those observed in stellar mass BHBs, but in an accretion state in which they are able to radiate at or even above the Eddington limit (see

* E-mail: dwalton@ast.cam.ac.uk

† E-mail: t.p.roberts@durham.ac.uk

Remillard & McClintock 2006 for a recent review of the standard BHB accretion states). A number of methods by which this may be physically possible have been suggested (see *e.g.* Poutanen et al. 2007; Finke & Böttcher 2007; Abramowicz et al. 1980). Indeed, observational evidence from ULXs now appears to show differences between ULXs and Galactic BHBs, suggestive of ULXs representing a new super-Eddington accretion state (Roberts 2007; Gladstone et al. 2009).

The third idea is that ULXs do not emit isotropically, and are sources that we view at a favourable orientation (King et al. 2001). Depending on the extent to which the emission is anisotropic, this can potentially lead to artificially inflated estimates for the luminosity of a source, which is usually calculated under the assumption of isotropy, and again there may be no need to invoke larger black holes than those present in stellar mass BHBs. In the context of ULXs, it has been suggested that the required anisotropic emission may be attained through *e.g.* geometric collimation of radiation due to a thick accretion disc (possibly the ‘slim’ discs proposed to allow super-Eddington emission, see Abramowicz et al. 1980), or through collimation into relativistic jets similar to those observed in other accreting sources (Reynolds et al. 1997). However, a growing number of ULXs are observed to be embedded within roughly spherically symmetric photoionised nebulae (Pakull & Mirioni 2003, Kaaret et al. 2004). Detailed study of these nebulae suggests they are not supernovae remnants (SNRs) but are apparently inflated by the ULX (Pakull & Grisé 2008). Strongly anisotropic emission may be ruled out in these cases through morphology and photon counting arguments, so it appears unlikely ULXs as a class may be considered ‘microblazars’.

We are now in the position where recent scenarios explaining the physical processes governing the high luminosities of ULXs combine two or more of the ideas presented above. For example, super-Eddington discs are predicted to inflate and produce outflowing winds that act to collimate the X-ray emission from their central regions (Begelman et al. 2006; Poutanen et al. 2007; King 2008). Also, it has been suggested that a proportion of the ULX population may consist of larger stellar remnant black holes (up to $\sim 80 M_{\odot}$), that may plausibly be formed in low-metallicity environments, accreting at mildly super-Eddington rates (Zampieri & Roberts 2009).

As previously stated, unambiguously distinguishing between these explanations, notably the IMBH and stellar mass interpretations, has proven extremely difficult on the basis of current observations. For a recent review on this topic, see Roberts (2007). In large part, this is because reliable dynamical mass estimates are not yet available for any ULXs. Until such mass estimates become reality, an excellent way in which to enhance our understanding of ULXs is through population studies of large ULX samples, as compiled by Colbert & Ptak (2002), Swartz et al. (2004), Liu & Bregman (2005) and Liu & Mirabel (2005). For example, such work has demonstrated that ULXs are strongly linked with recent star formation and are prevalently located in spiral galaxies (see *e.g.* Swartz et al. 2004; Grimm et al. 2003 and Gilfanov et al. 2004a; Liu et al. 2006; but especially Swartz et al. 2009 and references therein). This relationship with star formation strongly suggests that the majority of ULXs are a form of high mass X-ray binary (HMXB), where a massive young star forms the necessary large mass reservoir for the ULX (see *e.g.* Rappaport et al. 2005). It is also suggested that most of the ULXs observed in elliptical galaxies are likely to be low mass X-ray binaries (LMXBs; Colbert et al. 2004, Humphrey et al. 2003). Based on the luminosity function of a very large sample of HMXBs, and the relation between the star

formation rate and the total X-ray luminosity of star forming galaxies, Grimm et al. (2003) and Gilfanov et al. (2004b) argue that there may be an upper limit of $\sim 100 M_{\odot}$ to the black holes in standard HMXBs, which if true has important consequences for ULXs.

In addition, the compilation of large samples of ULXs can identify extreme examples of these sources. This is pertinent as it has become apparent that there exists a rare subgroup of the ULX population which display even more extreme X-ray luminosities of $L_X > 10^{41} \text{ erg s}^{-1}$. These have been dubbed Hyper-Luminous X-ray Sources (HLXs; Gao et al. 2003), and may be the most promising candidates in terms of the search for IMBHs. To date the most notable of these is ESO 243-49 HLX-1, observed to reach luminosities of $1.2 \times 10^{42} \text{ erg s}^{-1}$ (Farrell et al. 2009), but only a handful of other candidate HLXs are known (*e.g.* Davis & Mushotzky 2004; Jonker et al. 2010). Clearly finding more such objects is an interesting and potentially illuminating objective.

Here, we embark upon such a study and present a large catalogue of X-ray detections of candidate ULXs, compiled from Data Release 1 of the 2XMM Serendipitous survey (2XMM-DR1, hereafter referred to as 2XMM). The paper is structured as follows: section 2 details the observations used and the process of compiling the catalogue, section 3 presents and considers some of the science that may be derived from it, and finally section 4 summarises our conclusions.

2 CATALOGUE PRODUCTION

As stated, the major resource utilised for our source selection was the 2XMM-DR1 catalogue. This is described by Watson et al. (2009). In brief, this is a catalogue of 246897 detections drawn from 3491 public *XMM-Newton* fields imaged by the European Photon Imaging Camera (EPIC) detectors, data spanning the first 7 years of the mission. It contains 191870 unique X-ray sources (as some sources have been multiply imaged, given that *XMM-Newton* has studied some fields on several occasions), and covers roughly $\sim 1\%$ of the whole sky. Such a large catalogue presents a hitherto unrivalled opportunity to study relatively rare source classes such as ULXs; in fact, at the modal detection flux for a 2XMM source ($\sim 2 \times 10^{-14} \text{ erg cm}^{-2} \text{ s}^{-1}$ in the 0.2–12.0 keV band; see Fig. 9 of Watson et al. 2009) one can roughly expect to detect all isolated ULXs within the catalogue field-of-view out to $d \sim 20 \text{ Mpc}$. We therefore took the entire 2XMM catalogue as the starting point for our ULX candidate selection. This section describes the process of condensing 2XMM into a catalogue of ULX candidates, and the properties of the derived catalogue.

2.1 Initial Correlations and Filtering

The initial selection of ULX candidates was performed by cross-correlating the 2XMM catalogue with the Third Reference Catalogue of Bright Galaxies (RC3; de Vaucouleurs et al. 1991). This catalogue contains 23022 individual galaxies, the majority of which have either isophotal diameters $D_{25} > 1 \text{ arcminute}$, total *B*-band magnitude $B_T < 15.5$ or recessional velocity $cz < 15000 \text{ km s}^{-1}$. Before cross-correlation with 2XMM, galactic centre positions were updated and missing recession velocities obtained via a cross-correlation of RC3 with the online NASA Extragalactic Database (NED)¹ and the VIZIER/SIMBAD databases².

¹ <http://nedwww.ipac.caltech.edu/>

² <http://cds.u-strasbg.fr/>

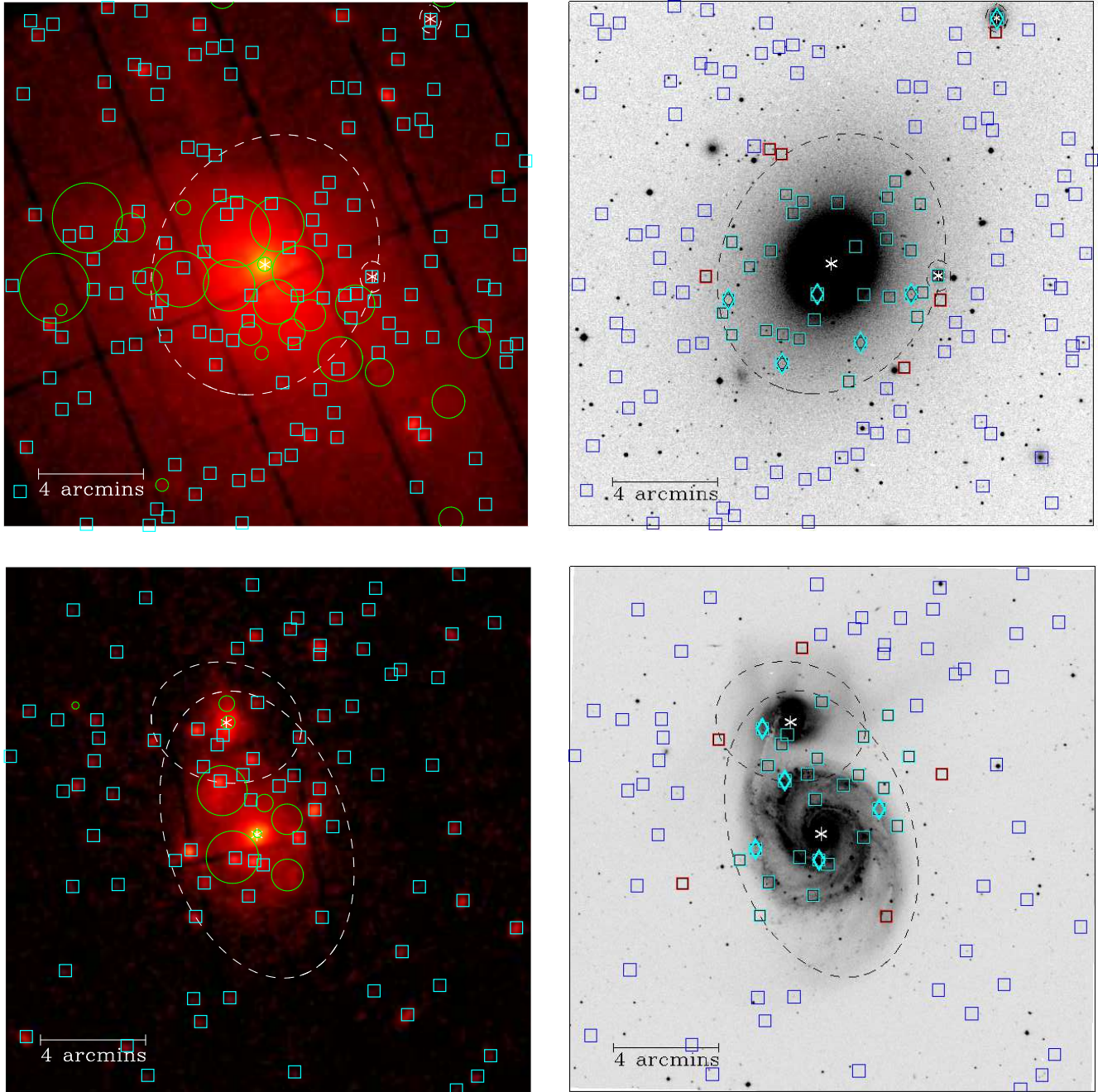


Figure 1. An illustration of the 2XMM data and ULX selection process. We show data for two galaxy fields: (*upper panels*) NGC 4472, also including NGC 4464 (to the north-west of NGC 4472, where north is up in all panels) and NGC 4467 (west of NGC 4472, overlapping its Σ_{25} ellipse); (*lower panels*) NGC 5194, overlapping with NGC 5195 to its north. In all panels the Σ_{25} isophotal ellipse is shown, and the galaxy nuclear position is marked with an asterisk. (*left panels*) A combined EPIC data broad-band (0.2–12.0 keV) image with source detections overlaid. The images were extracted as pipeline products from the *XMM-Newton* science archive (XSA), and are convolved with a 1-pixel ($\equiv 4$ arcsec) HWHM Gaussian mask for display purposes. The images are displayed on a logarithmic heat scale, between 2.5–100000 count pixel $^{-1}$ (NGC 4472), and 1–10000 count pixel $^{-1}$ (NGC 5194). Point source detections are marked by cyan open squares, and extended source detections by green circles with radius equivalent to the measured radius (note that this is capped at 80 arcsecs in the 2XMM catalogue). (*right panels*) Digitised sky survey (version 2) red images of the galaxy fields, with point source positions overlaid. Negative images, linearly scaled, are shown for display purposes. The catalogue creation process is highlighted by showing field sources as blue open squares, with sources within the Σ_{25} great circle but not the Σ_{25} isophotal ellipse shown by (thicker) red squares. Sources within the ellipses are shown as cyan open squares with black inner lining, with those selected at ULX-like luminosities highlighted by an additional diamond symbol.

Galaxies that remained without a recession velocity after these measures were excluded from our analysis. Distances to galaxies with recession velocities less than 1000 km s^{-1} , for which peculiar motions may dominate the Hubble flow, were obtained by cross-correlation with the nearby galaxy catalogue of Tully (1988). For the other galaxies, the Hubble flow is considered a good approximation, and distances were obtained using a Hubble constant of $H_0 = 75 \text{ km s}^{-1} \text{ Mpc}^{-1}$ to remain consistent with Tully (1988).

Cross-correlation of RC3 with 2XMM was performed using the TOPCAT graphical user interface³. An initial match was performed between 2XMM and RC3 via a conical search, within a radius equal to half of the RC3 galactic $\mathcal{Z}5$ semi-major axis (where the $\mathcal{Z}5$ ellipse is defined as the elliptical equivalent to the 25th magnitude isophote for a galaxy). An elliptical filter was then applied to the matched source list to select only those sources that lay within the $\mathcal{Z}5$ elliptical isophote of all the galaxies, based on the RC3 major and minor axis ratios and position angles. However, a number of galaxies included in RC3 do not have position angles listed. In these cases, we instead performed a circular match within the minor axis. At this point we also discarded all sources flagged as extended, as ULXs should by definition be point-like (although a more detailed discussion of this exclusion is given in section 2.5). The success of this process was verified by visual inspection for a number of galaxies; we show the examples of NGC 4472 and NGC 5194/5 in Fig. 1 for illustration, as well as to highlight the complexities and limitations of the 2XMM source selection process.

X-ray luminosities were calculated for all remaining sources using the full band EPIC flux (0.2–12.0 keV), as given in the 2XMM catalogue, and the distances to the putative host galaxies obtained earlier. The 2XMM fluxes are calculated separately for each of the three EPIC detectors from the observed count rates, assuming an absorbed powerlaw model for the average source spectrum ($\Gamma = 1.7$, $N_{\text{H}} = 3 \times 10^{20} \text{ atom cm}^{-2}$). The quoted EPIC flux is then the weighted average of the fluxes obtained for the individual detectors (Watson et al. 2009). Although luminosity uncertainties are likely to be dominated by the uncertainty in the distance to the galaxies, particularly where local peculiar motions may be important, the uncertainties in these distances are not well-quantified (although any error based on our choice of H_0 will at least be systematically propagated through the sample). We therefore calculated the uncertainty on the luminosity solely from the uncertainty on the flux. As dictated by the standard definition of a ULX, sources with $L_X < 10^{39} \text{ erg s}^{-1}$ were discarded, although those that were consistent within 1σ of such luminosities were retained in order to include the largest number of possible ULX candidates. We also adopted a slightly conservative stance on the quality of detection to retain, requiring them to be at least 3.5σ detections according to 2XMM. This analysis resulted in a large preliminary catalogue of source detections at (or above) ULX luminosities, and a small sample of slightly fainter X-ray sources.

2.2 Filtering for Known Contaminants

The largest identifiable contaminant of our sample of ULXs were the active galactic nuclei (AGNs) within the ULX host galaxies. A simple cut to remove classic AGNs at $L_X \geq 10^{42} \text{ erg s}^{-1}$ would however be insufficient for our purposes as it would not remove the potential low-luminosity AGNs (LLAGNs) contaminating our

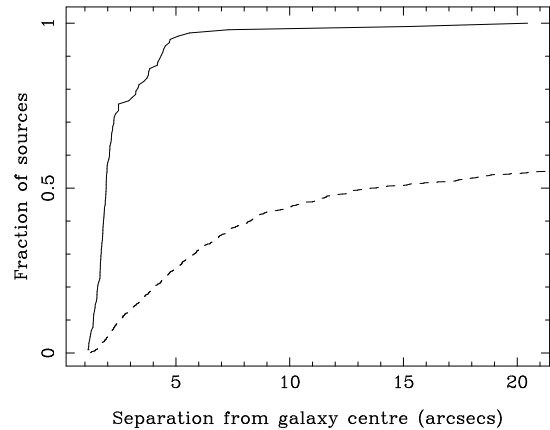


Figure 2. Cumulative distribution plot, showing the separation of the filtered 2XMM detections from the centres of the host galaxies. We plot this only for sources in close proximity to the nucleus ($r_{\text{max}} \lesssim 20$ arcsecs), and show the sample of classic AGNs (solid line), and the comparison ULX/LLAGN sample (dashed line) distributions separately.

sample. Unfortunately, LLAGNs overlap significantly with ULXs in terms of observed luminosity, with LLAGN luminosities as low as $\sim 10^{38} \text{ erg s}^{-1}$ (Ghosh et al. 2008; Zhang et al. 2009), hence making ULXs and LLAGNs indistinguishable by X-ray luminosity alone. The only way to circumvent this problem is to remove all possible LLAGN candidates; hence we were required to remove all sources in close proximity to the nucleus.

Their key question then is: what exclusion radius around the centre of the galaxy will optimise the removal of LLAGN candidates, while retaining the maximum number of ULXs? We approached this in an empirical fashion by defining a conservative maximum separation of each source from the nuclear position, r_{max} as the sum of its calculated separation and the 3σ error in its position as defined in 2XMM. We then selected the classic AGN contamination of the sample by discarding any sources with $L_X < 10^{42} \text{ erg s}^{-1}$, leaving 102 likely *bona fide* AGNs. We plot the separation of these sources (quantified as the maximum separation, r_{max}) from their host galaxy central position as a cumulative distribution in Fig. 2. The same distribution for all sources with $10^{39} < L_X < 10^{42} \text{ erg s}^{-1}$, taken from the same working version of the catalogue, is also shown in Fig. 2 in order to illustrate how any empirical cut would affect this section of the dataset.

The initial cut was taken at $5''$, as this removed 95% of the AGN sample, but only 25% of the sources with luminosities in the ULX range. As a significant fraction of the latter sample are likely to be LLAGNs, the number of actual ULXs discarded is unlikely to have been too large. However, an inspection of the remaining catalogue revealed that there were still a significant number of known and probable AGNs present. We therefore tried larger excision radii, and found that a value of $r_{\text{max}} = 7.5''$ struck the best balance between removing known AGNs and leaving a large sample of ULX candidates ($< 40\%$ of the ULX-luminosity sample are removed, many of which we suspect to be LLAGNs at these small nuclear separations).

The remaining sample was further cleaned with the following steps. Firstly, all high luminosity sources ($L_X > 10^{40} \text{ erg s}^{-1}$) were inspected by checking their host galaxy nuclear classification, their separation from the galaxy centre, and the size of their position error. We identified further examples of AGNs that had not been filtered by the excision radius due either to a poorly-defined nuclear position for the galaxy, or to a large position error, with the

³ Tool for Operations on Catalogues and Tables; <http://www.star.bris.ac.uk/~mbt/topcat/>

Table 1. Some brief details of the detections included in, and the host galaxies contributing to, the presented catalogue and some of its key subsets. Notes: both the average X-ray flux \tilde{f}_X , and the average total counts per source (summed across all three EPIC detectors) \tilde{C} , are given as the median value across all ULX candidate detections. All other averages are the arithmetic mean, and are shown with the calculated error on this value. The average X-ray flux and luminosity values are for the full 0.2–12.0 keV energy band.

	Full catalogue	Spiral sample	Elliptical sample	Complete sample
Total detections	650	450	200	242
Individual candidate ULXs	470	305	165	169
(with multiple detections)	101	70	31	31)
Host galaxies	238	141	97	71
(with multiple candidate ULXs)	113	79	34	43)
		<i>per host galaxy</i>		
$\langle d \rangle$ (Mpc)	37.9 ± 2.2	29.9 ± 2.1	49.6 ± 4.0	13.1 ± 0.7
$\langle M_B \rangle$	-20.5 ± 0.1	-20.3 ± 0.1	-20.7 ± 0.1	-20.2 ± 0.1
		<i>per ULX candidate detection</i>		
\tilde{f}_X (erg cm ⁻² s ⁻¹)	4.2×10^{-14}	4.8×10^{-14}	3.3×10^{-14}	1.4×10^{-13}
\tilde{C} (ct)	293	314	279	1160
$\langle \log L_X \rangle$ (erg s ⁻¹)	39.48 ± 0.02	39.46 ± 0.02	39.54 ± 0.04	39.31 ± 0.03
$\langle \text{HR1} \rangle$	0.48 ± 0.01	0.52 ± 0.02	0.41 ± 0.03	0.55 ± 0.02
$\langle \text{HR2} \rangle$	0.23 ± 0.01	0.26 ± 0.02	0.16 ± 0.03	0.30 ± 0.02
$\langle \text{HR3} \rangle$	-0.27 ± 0.01	-0.23 ± 0.02	-0.36 ± 0.02	-0.22 ± 0.02
$\langle \text{HR4} \rangle$	-0.46 ± 0.01	-0.46 ± 0.02	-0.45 ± 0.03	-0.50 ± 0.01

latter resulting from the source being weakly detected and/or well off-axis and/or in a region with a high diffuse background component; these were also discarded. There were also a number of high luminosity sources close to (within $\sim 15''$ of) the centres of elliptical galaxies that were not classified as AGNs. A conservative stance was also taken with these objects, many of which were poorly parameterised due to the presence of a strong diffuse ISM in the galaxies, as we were concerned the 2XMM catalogue may not be differentiating between peaks in the strong ISM and true point sources, hence these sources were also excluded. The second step related to sources that were multiply-detected in 2XMM, where only some detections lay within the $r_{\text{max}} = 7.5$ arcsec excision radius (which again was mainly due to poorer position constraints on some detections). All detections of these sources were excluded from the catalogue.

These measures remove the contamination of the sample by AGNs associated with the host galaxies. However, other AGNs may still be present in the field of view, predominantly at cosmic distances behind the host galaxies, some of which will be known objects. We therefore cross-correlated our remaining catalogue with the NED and SIMBAD/VIZIER databases to search for known QSOs and other potential contaminants. We found a total of 54 detections of 39 suspected contaminants coincident with our host galaxies, including 17 AGNs, 7 foreground stars and 13 possible X-ray detections of recent supernovae within the host galaxies. All these detections were discarded from our catalogue. Of course, this analysis will not correct for any previously *unknown* contamination of the sample with background or foreground objects, the magnitude of which was relatively large in previous ULX samples. We return to this problem in §2.4.

Finally, there were a number of other minor issues that required attention during the production of the cleaned catalogue. Close inspection revealed a number of repeated entries of the same detection of individual sources. This occurred where the source position lay under the 25 ellipse of multiple galaxies (see Fig 1 for some examples). In this situation we assumed the source was truly associated with the galaxy whose centre it was closest to, and removed all other entries of the same detection. In addition, we also

inspected the combined EPIC images of detections with small separations from their respective galactic centres to remove detections within the pattern of scattered light produced by the mirror supports for bright sources, which are likely to be artificial.

Once we had our catalogue of good ULX candidates, we returned to 2XMM to re-append any detections of these sources that had previously been discarded. This allowed for sources with variable luminosity, sources located right at the edge of the 25 isophote of their respective galaxies with detection positions scattered on either side, *etc.* It is after this analysis and filtering procedure that we present the catalogue.

2.3 The Catalogue

The filtering processes left us with a catalogue comprising of 650 detections of 470 individual candidate ULXs, 101 of which were detected on two or more occasions. Of the detections included, 121 have $L_X < 10^{39}$ erg s⁻¹, of which 79 are within 1σ of the classic ULX luminosity limit; the rest are detections of sources with variable luminosity which have been observed to emit at $L_X > 10^{39}$ erg s⁻¹ at other epochs. The catalogue contains 369 data entries per candidate ULX detection, including the full RC3 entry for the host galaxy, the full 2XMM entry for the X-ray source, and additional information we have added in the derivation of the catalogue (distance, X-ray luminosity, *etc.*). For ease of comparison, we highlight probable common entries between our catalogue and those of Colbert & Ptak (2002), Swartz et al. (2004), Liu & Bregman (2005) and Liu & Mirabel (2005). The catalogue contains 367 sources that do not appear to be in any of those works, that we flag as ‘new’ ULX candidates. The position errors on the detections are on average only $1''$, and are always less than $3.5''$. Additional summary details of the catalogue are presented in Table 1, as well as a detailed example of some catalogue entries in Appendix A. The full catalogue itself is available electronically with this paper⁴.

⁴ Catalogue to be made available online via MNRAS; available in the meantime via private communication

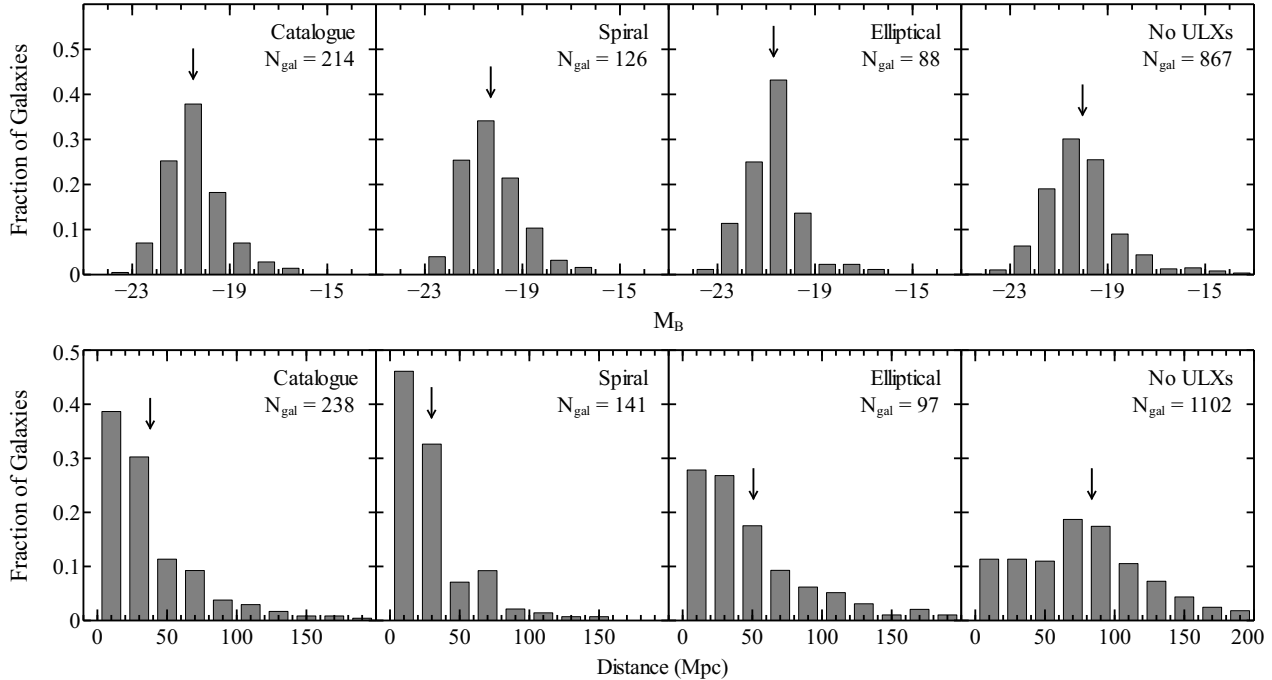


Figure 3. Fractional distributions for the absolute B band magnitude (magnitude bins) and the distance (20 Mpc bins) for RC3 galaxies that host ULX candidates. Arrows indicate the values quoted in Table 1. Elliptical galaxies are in general brighter, and more distant than their spiral galaxy counterparts. For comparison, we also show the distributions of the RC3 galaxies covered by 2XMM-DR1 observations that did not contribute any ULX candidates to our sample. Note that the gaps in the histograms are for aesthetic purposes only, and that not all RC3 galaxies have B-band magnitude entries.

In this section, and much of the rest of this paper, we choose to treat the ULX candidates hosted by spiral galaxies and those hosted by elliptical galaxies separately. There are very clear reasons for making this separation. Previous work has shown that the X-ray source populations of galaxies are dependent on two factors: the mass of the galaxy, which relates to an underlying population of older LMXBs, and the amount of ongoing star formation, which relates to the HMXB population (e.g. Colbert et al. 2004; Humphrey et al. 2003; Lehmer et al. 2010). In terms of ULXs, it is clear that many of the ULXs in spiral galaxies - particularly in hosts with a high star formation rate - are directly related to the star formation and are likely a type of high-mass X-ray binary system (see Swartz et al. 2009 and references therein). This large-scale star formation is not present in elliptical galaxies, and so a separate, physically distinct type of ULX must be present in these systems, as argued by King (2002). We therefore distinguish elliptical and spiral candidate ULXs in our analysis, making the distinction based on the numerical index for the Hubble type, T , as registered in RC3. Candidate ULXs in types SO/a and later ($T \geq 1$) are taken to comprise the spiral sample (which therefore includes all morphologically irregular and peculiar systems), with the remainder of sources in hosts with $T < 1$ constituting the elliptical sample (which includes both elliptical and lenticular host galaxies).

Table 1 shows that we detect a factor of ~ 2 more ULX candidates in spiral galaxies than in ellipticals, and we have a slightly higher proportion of multi-epoch datasets for spiral candidate ULXs. We also have a factor ~ 2 more host spiral galaxies than ellipticals, although as shown in Fig. 3 the elliptical hosts have a mean distance $\sim 70\%$ greater than spirals, and also are on average bigger and brighter with a mean absolute magnitude nearly half a magnitude higher. The mean log X-ray luminosity of the candi-

Table 2. Energy ranges covered by the 2XMM energy bands.

2XMM Band	Energy (keV)
1	0.2–0.5
2	0.5–1.0
3	1.0–2.0
4	2.0–4.5
5	4.5–12.0

date ULX detections in each sample are approximately the same (see Fig. 4); however, given the greater distance to the ellipticals the candidate ULXs possess a fainter median X-ray flux. Despite this, we accumulate similar median numbers of X-ray photons per detection in both samples (also demonstrated in Fig. 4), since the elliptical galaxies typically have longer observations. Note that the values quoted in Table 1 are calculated for all the detections included in the catalogue, if we limit ourselves to detections above 10^{39} erg s $^{-1}$, the mean $\log(L_X)$ values increase to 39.61 ± 0.03 and 39.63 ± 0.04 for spiral and elliptical detections respectively, which are extremely similar.

Perhaps the most interesting distinction between the samples comes in terms of the 2XMM X-ray hardness ratios, defined as:

$$HR = \frac{C_B - C_A}{C_B + C_A} \quad (1)$$

where C_A and C_B are the count rates of the two bands under consideration. The energies covered by the five 2XMM energy bands

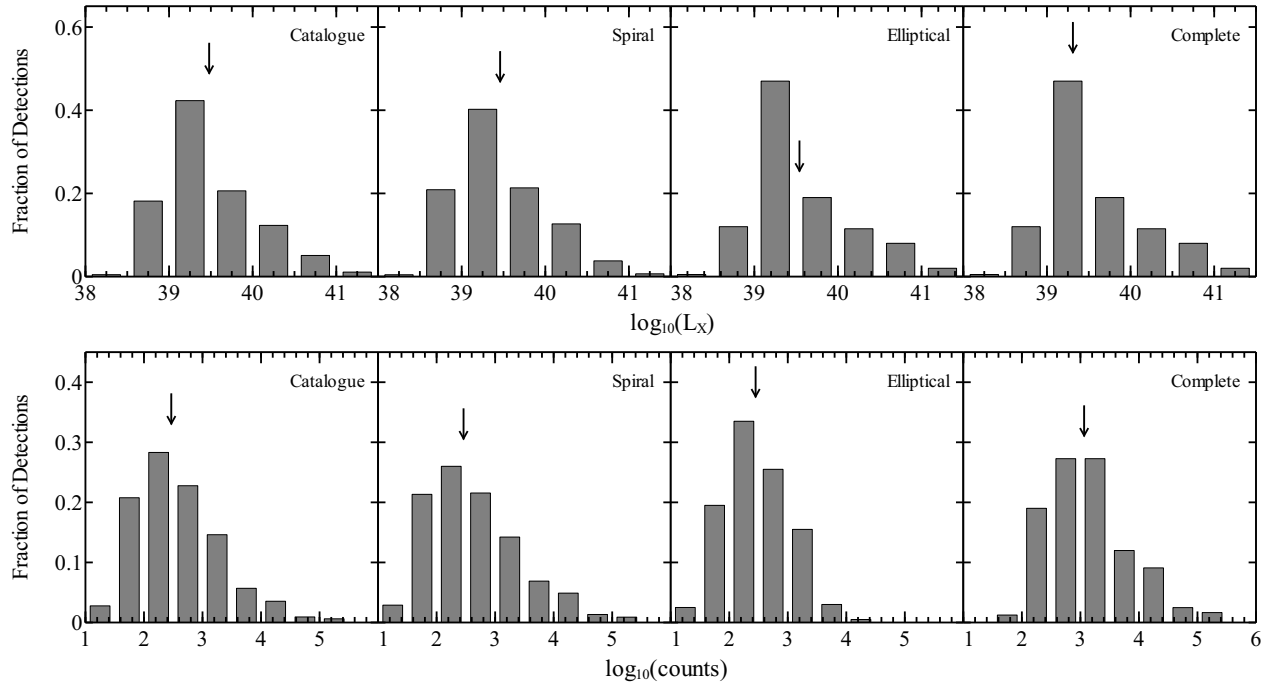


Figure 4. Fractional distributions for the X-ray luminosities and the number of photons detected from the ULX candidates (0.5 dex bins) included in the presented catalogue. Arrows indicate the values quoted in Table 1. The mean X-ray luminosity and the median numbers of counts received are similar for detections associated with spiral and elliptical galaxies.

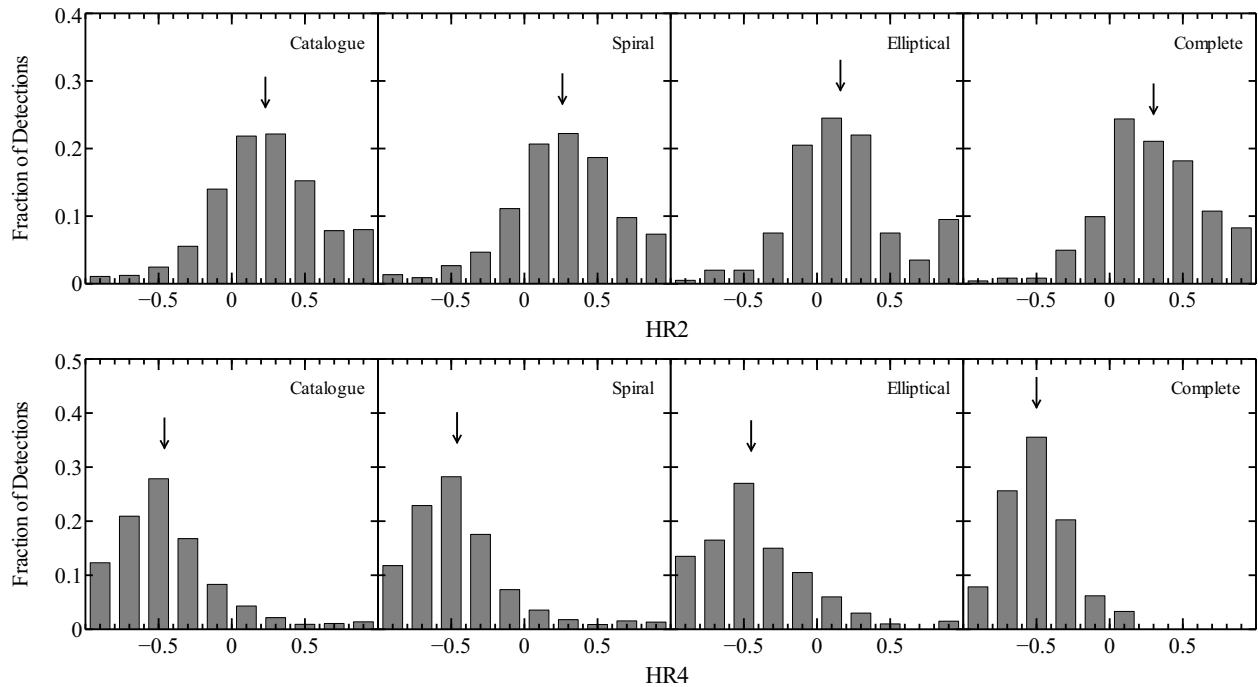


Figure 5. Fractional distributions for the 2XMM EPIC hardness ratios HR2 and HR4 ($\Delta HR = 0.2$ bins) for the ULX candidates included in the catalogue. Arrows indicate the values quoted in Table 1. Detections from spiral galaxies appear harder at low energies than their elliptical counterparts, but this discrepancy is not seen at higher energies. This may be an indication that the sources in spiral galaxies are more absorbed.

are given in Table 2; HR1 combines bands 1 and 2, HR2 combines bands 2 and 3, *etc.* The 2XMM hardness ratios are normalised to be in the range $[-1, 1]$ with harder spectra having more positive hardness ratios. Although Fig. 5 shows the detections display a wide range of hardness ratios, the mean hardness ratio values are constrained to about ± 0.02 in each case; hence the differences between the spiral and elliptical sample are significant at the $\sim 3 - 4.5\sigma$ level for hardness ratios HR1, HR2 and HR3. In each case the spiral hardness ratio indicates the sources are somewhat spectrally harder than their elliptical counterparts, with this spectral distinction not apparent in HR4. To demonstrate this we show the number distributions of HR2 and HR4 in Fig. 5 for both the elliptical and spiral galaxy detection populations. The difference in the mean values for HR2 is largely driven by an absence of detections with hard spectra below 2 keV from elliptical galaxies. We suggest this may primarily be due to the presence of more neutral gas in spiral galaxies, particularly in the star-forming regions hosting the ULXs, which will lead to more absorbed and hence harder spectra. However, a higher column physically associated with each ULX in spiral galaxies - perhaps a result of mass-loss from the likely high-mass stellar secondaries in such systems - is also an intriguing possibility. Whatever the cause, this difference supports the decision to separate our candidate ULXs into two distinct samples.

Within the catalogue there are also 5 sources that appear to display HLX luminosities, none of which have previously been included in ULX catalogues to date. The brightest of these is 2XMM J134404.1-271410, which was observed at $L_X = (2.82 \pm 0.24) \times 10^{41} \text{ erg s}^{-1}$. However the closest HLX included in our catalogue, and hence potentially the easiest to study, is 2XMM J011942.7+032421 (hereafter NGC 470 HLX1), associated with the relatively nearby ($d \simeq 34 \text{ Mpc}$) spiral galaxy NGC 470. This source was observed to reach a luminosity of $L_X = (1.53 \pm 0.08) \times 10^{41} \text{ erg s}^{-1}$. These sources will be the subject of forthcoming work (Sutton et al. 2010; Sutton et al. in prep.), which will include recently obtained follow-up observations of NGC 470 HLX1.

2.3.1 The complete sub-sample

In order to undertake certain statistical studies of the population, it is necessary to define a ‘complete sample’, *i.e.* the subset of the catalogue compiled from observations of galaxies in which all the ULX candidates present within that galaxy should be detected. By doing so, we avoid including an artificial bias for brighter sources. Note that in this context we consider an observation of a galaxy to be complete if it is possible to detect all the sources that match our selection criteria; this does not address the limitations with respect to completeness inherent within these criteria, which are discussed in §2.5.

To determine whether an observation of a galaxy can be considered complete there are two limiting flux sensitivities that must be considered and compared. The first is the sensitivity of the observation, f_{obs} , *i.e.* the minimum count rate that a source must have to be detected at a certain position in the detector with a given detection significance. This value is mainly determined by the local effective exposure and background level. In order to compute a sensitivity map for each *XMM-Newton* observation in the soft (0.5–2.0 keV) and hard (2.0–12.0 keV) bands we used an empirical approach (see Carrera et al. 2007 and Mateos et al. 2008 for a detailed description of the method). Briefly, if Poisson statistics hold, it is possible to determine the minimum count rate that a source must have to be detected with a given significance. This Poissonian count rate is calculated from the total number of background counts and mean

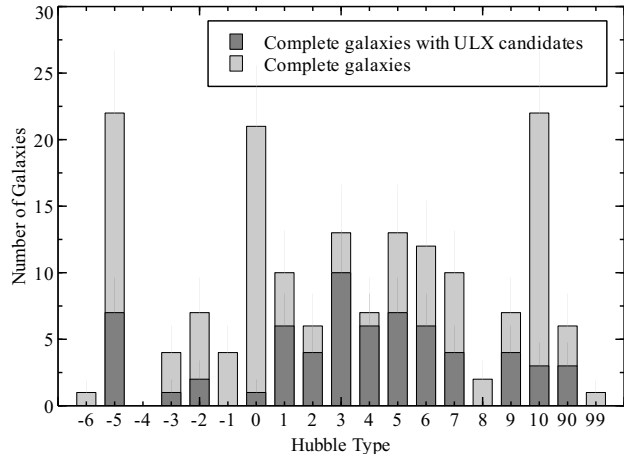


Figure 6. Number distributions of the Hubble type for all galaxies with complete observations, and galaxies with complete observations that host one or more ULX candidates. It is clear that ULXs are preferentially located in early type spiral galaxies.

effective exposure around the source position. However, source detection and parameterisation in the 2XMM pipeline is a complicated process that involves a simultaneous maximum likelihood fit of the distribution of source counts detected with each EPIC camera in different energy bands convolved with the telescope’s point spread function (PSF). Therefore the count rate values resulting from the source detection process are bound to deviate from the assumption of pure Poissonian statistics. However, as it is shown in Carrera et al. (2007) and Mateos et al. (2008), there exists a linear relationship between Poissonian count rates and those derived from the *XMM-Newton* pipeline. This relationship can be used to empirically correct the pipeline count rates from all non Poissonian effects. This approach is used by the Flux Limits from Images from *XMM-Newton* (FLIX) server provided by the *XMM-Newton* Survey Science Centre (SSC)⁵. Throughout this work, we utilise sensitivity maps calculated for a 5σ detection significance.

The second is the flux of a source emitting at $10^{39} \text{ erg s}^{-1}$ at the distance of the galaxy in question, which we refer to as the ULX luminosity limited sensitivity, f_{ulx} . In order to consistently compare f_{obs} and f_{ulx} , we calculate f_{ulx} for the full *XMM-Newton* bandpass (0.2–12.0 keV), then distribute the sensitivity between the hard and soft bands according to an average ULX spectral shape. We adopt a simple absorbed power-law model, with $\langle \Gamma \rangle = 2.2$ and $\langle N_H \rangle = 2.4 \times 10^{21} \text{ atom cm}^{-2}$, determined from the sample presented in Gladstone et al. (2009). Using PIMMS⁶ we find that approximately 36 per cent of the flux from ULXs should be observed in the soft band.

Having calculated f_{ulx} for each energy band, we compare this with f_{obs} for each observation of each galaxy across its projected area (excluding chip gaps, *etc.*, as well as the circular region of radius 7.5” excluded from our analysis during our consideration of nuclear sources). This comparison is performed separately for the EPIC-pn and two EPIC-MOS detectors. An observation of a galaxy in a particular band with a particular detector is considered complete if f_{ulx} is greater than f_{obs} for the whole of the considered galaxy area. We take an observation of a galaxy to be complete in

⁵ <http://www.ledas.ac.uk/flix/flix.html>

⁶ <http://heasarc.nasa.gov/docs/software/tools/pimms.html>

general if it can be considered complete in either of the bands for any of the detectors, as regardless of whether it is complete for only one band in one detector or both bands in all detectors, all the ULXs detectable with our selection criteria should appear in the catalogue. On investigation, we find that any observation that is considered complete in the hard band is always considered complete in the soft band as well.

The complete sub-sample consists of 242 detections of 169 discrete sources, including 130 sources which are observed to radiate at or in excess of 10^{39} erg s⁻¹. Of these, 106 are found in 52 spiral galaxies, and 24 in 12 elliptical galaxies. The spatial coverage of 2XMM includes complete observations of a total of 108 spiral and 56 elliptical RC3 galaxies (i.e. galaxies for which the completion criteria are met, regardless of whether they actually host a ULX candidate). In Fig. 6 we show the number distributions of the Hubble type for all the galaxies with complete observations, as well as those with complete observations that host ULX candidates. It is clear that ULXs are preferentially located in early type spiral galaxies, as would be expected given the association between ULXs and regions of high star formation (Swartz et al. 2009). The lack of ULX candidates in elliptical galaxies is a consequence of their relatively low star formation rates, while the lack of ULX candidates in late type spirals arises due to the majority of these being dwarf galaxies, which do not contain enough stellar mass to host ULXs. Of the 169 sources included in the complete sample, 106 are ‘new’ detections, of which 71 are observed to radiate at or in excess of 10^{39} erg s⁻¹. Finally, there are also 39 sources included that are not observed to radiate at $L_X \geq 10^{39}$ erg s⁻¹ at any epoch contributing to the complete sample, although 8 of these sources are observed at ULX luminosities at other epochs that contribute only to the general catalogue. These fainter sources are also primarily observed in spiral galaxies, with only 7 of the 39 associated with ellipticals.

In Table 1 and Figures 4 and 5 we provide a comparison of the complete subsample and the catalogue as a whole. As expected, the mean distance to host galaxies for the complete sample is significantly smaller than that of the catalogue as a whole (all galaxies with complete observations are within 24 Mpc), and the host galaxies are fainter on average. In addition, although the detections in the complete sample typically have many more counts, their average luminosity is lower than that of the whole catalogue. This arises naturally from the fact that a large portion of the detections in the full catalogue arise from observations of galaxies that did not have the sensitivity to detect sources at 10^{39} erg s⁻¹. Consequently, there is a slight bias towards brighter sources in the full catalogue, which is not present in the complete subsample. Finally, there are also some slight differences in the average hardness ratios between the complete sample and the full catalogue, which will be discussed in more detail in forthcoming work (Walton et al. in prep.).

2.4 Estimating the Contribution from Unknown Contaminants

When producing a catalogue of any specific astronomical object it is important to consider what fraction of the sources included are likely to be undesirable contamination, e.g. background quasars in this case. Here we attempt to quantify the expected contribution from such unknown contaminants. In brief, this requires estimation of the number of background sources that should be observed at some minimum detection significance (for *all* RC3 galaxies observed), and comparing this with the actual number of sources detected at or above that minimum significance. Like the consid-

eration of observation completeness, our calculations have been performed separately for each EPIC detector in the soft and hard bands, as dictated by the availability of the sensitivity maps.

Since the catalogue compiled is of sources with $L_X > 10^{39}$ erg s⁻¹, only background contaminants with apparent luminosities also in this range needed to be considered, so we again make use of the full band f_{ulx} calculated previously. However, we are now considering a different class of source, most likely background quasars, which on average may not have their flux distributed between the soft and hard bands in the same way as ULXs. Piconcelli et al. (2003) find that observed spectra of the majority of background quasars are adequately modelled with a powerlaw continuum, modified by Galactic absorption, so we again adopt a simple absorbed power law model for the average spectral shape of background sources. In this calculation we use the average photon index of $\langle \Gamma \rangle = 1.59 \pm 0.02$ obtained by Piconcelli et al. (2003) and the Galactic column density in the direction of each galaxy (Kalberla et al. 2005). For each galaxy the fraction of the 0.2–12.0 keV flux that should be observed in the soft and hard bands (0.5–2.0 and 2.0–12.0 keV respectively) was determined using PIMMS, and f_{ulx} was recalculated for each band accordingly. On average ~30 per cent of the flux from these sources should be observed in the soft band. We again compare these sensitivities to the observation sensitivities provided by the sensitivity maps, f_{obs} . The true limiting sensitivity f_{lim} relevant to this calculation is whichever of these two is greater, as expressed by equation 2:

$$f_{lim} = \begin{cases} f_{ulx} & f_{ulx} > f_{obs} \\ f_{obs} & f_{ulx} < f_{obs} \end{cases} \quad (2)$$

Adopting this form simultaneously accounts for observations of galaxies deep enough to detect sources fainter than ULXs, and observations in which not all the ULXs in a galaxy could be detected. Using equation 2, modified sensitivity maps of f_{lim} were generated.

It has long been known that the majority of the Cosmic X-ray Background (CXB) can be accounted for by emission from discrete sources, as summarized in Hasinger (2004). Moretti et al. (2003) investigated the number of such sources that should be resolved ($N(>S)$, per unit sky area) as a function of flux sensitivity, S , finding that this was well modelled as a smooth broken power law in both the hard and soft bands (note that the hard band used in Moretti et al. 2003 only covers 2.0–10.0 keV, however we expect that any corrections due to the slight differences in energy range between their hard band and the hard band used here will be minimal, so it should still be acceptable to compare the two). These relations were used to convert our limiting sensitivity maps into maps of the number of background contaminants expected from each pixel (one pixel covers a 4×4 arcsec area of the sky). The total background contribution from each galaxy was taken as the sum of all the individual pixel contributions that fell within their 25 isophote (again excluding the nuclear region, chip gaps, etc.), and the total background contribution expected in the catalogue was then the sum of the contributions from all the RC3 galaxies covered by observations included in 2XMM. Where galaxies have been observed on multiple occasions, only the contribution from the deepest observation was considered.

In order to compare the number of expected background sources with the number included in the catalogue we generated hard and soft band maximum likelihoods (MLs) using those given for the five basic energy bands included in 2XMM. We make the

Table 3. Fractional background contamination estimates calculated for the hard and soft bands for the PN and MOS detectors (see text). The analysis is also broken down into separate considerations of the catalogue subsets from spiral and elliptical type galaxies, as well as the complete sub-sample.

	Estimated Contamination (%)					
	Soft	Hard	Soft	Hard	Soft	Hard
	All Galaxies		Spiral Galaxies		Elliptical Galaxies	
PN	33.9 ± 4.6	12.9 ± 3.7	28.3 ± 4.8	10.8 ± 3.5	46 ± 10	19 ± 10
MOS1	35.8 ± 5.1	19.5 ± 4.2	29.9 ± 5.5	12.8 ± 4.0	47 ± 11	39 ± 12
MOS2	37.1 ± 5.4	18.5 ± 4.1	28.8 ± 5.3	12.5 ± 4.0	58 ± 14	35 ± 11
Weighted Average	24.0 ± 4.1		17.9 ± 3.8		39 ± 5	
	All Complete Galaxies		Complete Spiral Galaxies		Complete Elliptical Galaxies	
PN	32.9 ± 6.6	14.0 ± 4.6	28.0 ± 6.5	11.8 ± 4.5	54 ± 21	23 ± 15
MOS1	37.2 ± 7.3	17.9 ± 5.0	31.9 ± 7.3	14.1 ± 4.9	58 ± 22	34 ± 17
MOS2	35.8 ± 7.1	17.5 ± 5.0	30.5 ± 7.1	13.8 ± 5.0	57 ± 22	32 ± 16
Weighted Average	22.5 ± 4.4		18.5 ± 4.0		39 ± 6	

approximation that the hard and soft ML values are the sum of the likelihoods of the basic band they each encompass, which is increasingly good for higher detection likelihoods. We then counted the number of sources (note that we counted *sources* rather than detections, as we only considered the deepest observation for galaxies observed multiple times) with a detection significance of at least 5σ ($ML > 15$). These were compared with the number of estimated background sources calculated previously to obtain fractional contamination estimates for each band and each detector, after taking into account the known background contaminants already removed (see §2.2). Our estimates are given in Table 3, with quoted uncertainties based on counting statistics. We also present the results of the same calculation for the complete sub-sample of the catalogue, as defined in §2.3.1.

The average contamination is found to be ~ 24 per cent, similar to that estimated for previous ULX catalogues (Swartz et al. 2004). It is clear from Table 3 that the subset of detections associated with elliptical galaxies should be significantly more contaminated by unidentified background sources than the detections associated with spiral galaxies. Such a result may have been expected given the known observational characteristics of the ULX population which, as highlighted in §2.3, are also reflected in this catalogue. ULXs are often associated with star forming regions (Swartz et al. 2009), which are more common to spiral galaxies than elliptical galaxies, hence ULXs are more commonly observed in spiral galaxies. In addition, the observed elliptical galaxies are in general both larger and further away than the observed spiral galaxies, hence covering a greater cumulative area on the sky at lower ULX-detection fluxes. This combination leads naturally to a higher estimation of the fractional contamination.

Finally, we note briefly that the average contamination estimates presented in Table 3 may be better considered as upper limits to the fractional contamination rather than true predictions of the likely value. This is because our calculation does not correct for the flux extinction that will be suffered by background sources due to the gas and dust in the galaxies these sources are falsely associated with. Such considerations are especially relevant for spiral galaxies, which should contain higher columns of neutral gas and dust than their elliptical counterparts, as suggested by the hardness ratio comparison discussed in section 2.3. As such, although we quote values based on the calculations for both the soft and hard bands to

be conservative, the contamination estimates for the hard band, in which effects due to absorption will be greatly reduced, are likely to be more representative of the true contamination. This is therefore likely to be closer to ~ 17 per cent for the whole catalogue, and as low as ~ 12 per cent for the spiral galaxy population.

2.5 Limitations of the Catalogue

The largest dedicated catalogue of ULX candidates compiled to date is presented in Swartz et al. (2004), and includes 154 discrete sources with an estimated 25 per cent background contamination. The catalogue presented here, with 475 sources and at most a similar contamination represents a significant improvement in number⁷, and should provide a useful resource for the ongoing investigations into the properties of the ULX population; see §3 for examples of possible analyses that may be performed. However, before embarking upon any such study it is important to consider the limitations of this catalogue.

The fractional contamination could be further reduced by highlighting and removing additional contaminants with multi-wavelength observations and correlations. Such analysis is beyond the scope of this paper, but could be performed in future work involving follow-up observations. Wong et al. (2008) present an example of highlighting background AGNs with optical observations, but spectra from other wavelengths could also be used to detect characteristic features of AGNs, e.g. broad and narrow emission lines from Seyfert galaxies.

Perhaps the major limitation on this catalogue is its incompleteness. There will inevitably be a population of ULXs residing in the galaxies observed that are not included in this catalogue. Obviously the observations of some galaxies were not deep enough to detect all the sources down to 10^{39} erg s⁻¹. In addition, a number of legitimate ULXs will have been discarded in the empirical

⁷ Since this work was submitted, a large catalogue of general X-ray point sources in nearby galaxies has been published by Liu (2011), compiled from *Chandra* observations. That catalogue contains 300 candidate ULXs within the D₂₅ galaxy regions, and an additional 179 candidates in the region between the D₂₅ and 2D₂₅ ellipses, although we caution that a large fraction (~ 60 per cent) of the latter sample are likely to be contaminants.

nuclear cut and by discarding extended sources. In terms of the latter reason, star forming regions often appear as diffuse, extended emission and due to their well documented association with these regions it is likely some ULXs will be embedded within them. With its fairly modest spatial resolution, *XMM-Newton* can have difficulty resolving ULXs in this situation, so by excluding extended sources we are also excluding any ULXs that may be ‘hidden’ within them. A particularly good example of this problem for *XMM-Newton* is the relatively nearby ($d \sim 35$ Mpc), intense star forming galaxy NGC 3256. *XMM-Newton* observations reveal an extended X-ray emission region centred on the galaxy, with a solitary ULX outside this region (Jenkins et al. 2004), whereas *Chandra* has resolved the central regions to reveal a population of ULXs embedded within regions of strong diffuse emission (Lira et al. 2002). In addition, detections that appear as extended with *XMM-Newton* may actually be emission from an unresolved population of point sources. This may even be the case for a number of detections that appear as point sources with *XMM-Newton*, a possibility which becomes increasingly likely for more distant galaxies. The combination of these effects is difficult to quantify, but the net result is likely to be that there are additional ULXs in some of the galaxies observed that are not included in this catalogue, even for galaxies that have observations we have considered as ‘complete’. Observations of these galaxies with *Chandra* should go some way to addressing these issues, owing to its significant improvement on the angular resolution of *XMM-Newton*.

3 EXAMPLE APPLICATIONS OF THE CATALOGUE DATA: ANALYSIS AND DISCUSSION

In order to demonstrate the scientific potential a resource such as this catalogue offers, we now present a brief analysis highlighting some characteristics of the derived population based on an analysis of the statistically complete sample. We note that the main advantage enjoyed by the 2XMM catalogue over comparable resources is the higher photon statistics per detection, enabling more detailed studies of source characteristics over a broader energy range. This will be explored in future work (Walton et al. in prep.).

3.1 Luminosity Function

One way in which we may investigate the ULX population is through construction of its luminosity function. In order to avoid the estimation of corrections to account for incompleteness, we make use of the previously defined complete subset of the presented catalogue, for which such corrections should not be necessary, or at least negligible (even these data may suffer from some level of incompleteness as we are limited by the *XMM-Newton* angular resolution; see §2.5). There are a number of galaxies contributing to the complete sample that are found to have multiple observations that can be considered complete. Although there is some evidence that X-ray luminosity functions don’t change significantly from epoch to epoch, even if the sources contributing are variable (see *e.g.* Zezas et al. 2007), we adopt a conservative stance and only consider the longest observation of each galaxy.

These observations contribute 121 discrete sources radiating at or above 10^{39} erg s⁻¹. We group these into equally spaced 0.1 dex logarithmic luminosity bins, with the uncertainty on the number of sources in each bin given by Poisson counting statistics. Us-

ing the SHERPA modelling package⁸, we fit the luminosity function by minimizing a form of the Cash statistic (C ; Cash 1979) adapted to be an analogue to χ^2 (*i.e.* a reduced statistic of $C_\nu \sim 1$ for acceptable fits), and find that the data are well modelled with a single power-law up to the highest luminosity sources in the complete sub-sample ($L_X \simeq 5.5 \times 10^{40}$ erg s⁻¹); the differential and integral forms of such a relation are given in equations 3 and 4:

$$\frac{dN}{dL_X} \propto L_X^{-\alpha} \quad (3)$$

$$\Rightarrow N(> L) \propto L_X^{-(\alpha-1)} \quad (4)$$

This simple model gives a reduced statistic of $C_\nu = 0.89$, with the best fit value of the exponent $\alpha = 1.96 \pm 0.11$ (here and throughout this section quoted uncertainties are the 1σ uncertainties on one parameter of interest). On investigation, we find that the quality of fit, and the exponent obtained are not dependent on our choice of luminosity bin size. In Fig. 7 we show the integral form of the luminosity function (equation 4), rebinned so that there are approximately 5 additional sources from one luminosity bin to the next for clarity, and the best fit power-law model. The bin centroids in Fig. 7 are the average of $\log(L_X)$ for the additional sources included in each bin.

We also investigate the luminosity functions for the spiral and elliptical galaxy ULX populations separately. Of the 121 sources considered previously, 97 are located in spiral galaxies and 24 in elliptical galaxies. Again, we apply a simple power-law model to each, and find that this provides an excellent representation of the data in both cases ($C_\nu = 0.97$ and 0.7 respectively), with $\alpha_{\text{spiral}} = 1.85 \pm 0.11$ and $\alpha_{\text{elliptical}} = 2.5 \pm 0.4$. As with the full complete sample shown in Fig. 7, in Fig. 8 we show the integral forms of the spiral and elliptical luminosity functions, rebinned in a similar fashion. Although the exponents for spiral and elliptical galaxies agree within their 2σ uncertainties, due to the large uncertainty on the elliptical exponent, which in turn is a consequence of the relative lack of sources from those galaxies, there is a tentative suggestion that the luminosity function for sources in elliptical galaxies is steeper than for those in spiral galaxies. This would be consistent with the steepening of the elliptical luminosity function seen in the samples of Swartz et al. (2004) and Colbert et al. (2004). Such a result would not be surprising given the expectation that the sources in elliptical galaxies are likely to be LMXBs, while those in spiral galaxies are likely to be HMXBs (Colbert et al. 2004; Humphrey et al. 2003), and the shapes of the ‘universal’ luminosity functions compiled for these two classes of BHB, see Grimm et al. (2003) and Gilfanov (2004). The exponents obtained here are consistent within uncertainties with the relevant exponents for the HMXB and LMXB luminosity functions obtained in those works, both of which extend to luminosities below 10^{39} erg s⁻¹. This might suggest that the same process, or combination of processes, responsible for forming the lower luminosity BHB population are also responsible for forming the majority of ULXs.

It has previously been reported that there may be a high luminosity cut-off in the ULX luminosity function at $L_X \sim 2 \times 10^{40}$ erg s⁻¹, see *e.g.* Swartz et al. (2004) but especially Grimm et al. (2003) and Gilfanov et al. (2004b), who argue strongly for an upper limit to the luminosity of HMXBs. Given the large overlap between

⁸ <http://cxc.harvard.edu/sherpa/>

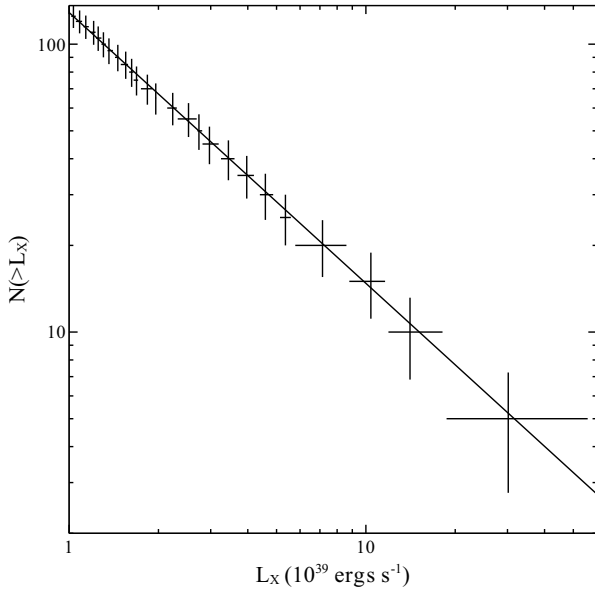


Figure 7. The luminosity function derived from the complete subset of the catalogue. The best fit single power-law model (see text) is also shown.

the ULX and HMXB populations this is also relevant for the ULX luminosity function. Such a cut-off may arise due to there being an upper limit to the mass of the black holes HMXBs are expected to contain, which Grimm et al. (2003) estimate to be $\sim 100 M_{\odot}$ under the assumption that the Eddington limit is not violated. Although the data are already reproduced well with a single power-law function, we also investigate a broken power-law model, as expressed in equation 5:

$$\frac{dN}{dL_X} \propto \begin{cases} L_X^{-\alpha_1} & L_X < L_c \\ L_X^{-\alpha_2} & L_X > L_c \end{cases} \quad (5)$$

However, this more complex model provides a negligible improvement in the fit to the data: we find $\Delta C = 0.1$ for 2 extra degrees of freedom, the break luminosity L_c is not well constrained (although its best fit value is $1.1 \times 10^{40} \text{ erg s}^{-1}$, similar to previously proposed values for L_c), and the two exponents are consistent within their 1σ uncertainties. Since the work of Grimm et al. (2003) focuses on HMXBs and Swartz et al. (2004) only see the cut-off in the luminosity function of spiral galaxies, we repeat the comparison using only the sources from complete spiral galaxies. Unsurprisingly, as our overall luminosity function is dominated by sources from spiral galaxies, we find exactly the same results, with an improvement now of $\Delta C = 0.2$ for 2 extra degrees of freedom.

We must remind and caution the reader that our luminosity functions are generated from sources from ensembles of galaxies. Although the broad, general shape should remain robust, non-systematic errors in the estimated luminosities that differ from galaxy to galaxy due to *e.g.* poorly estimated galaxy distances that could smear out complex features such as a cut-off. If present, the effect of such uncertainties would be especially prevalent at high luminosities where there are fewest sources. In this work we have adopted a simple Hubble Flow distance for galaxies with $cz > 1000 \text{ km s}^{-1}$ and the distance quoted in Tully (1988) for galaxies with $cz \leq 1000 \text{ km s}^{-1}$; a more careful analysis of galaxy distances, which is beyond the scope of this work, might clar-

ify this issue. Other biases may also be present too, for example background contamination. Removing these sources might alter the shape of the pure ULX luminosity function. However, a repeat of the work in §2.4 for sources with L_X above $5 \times 10^{40} \text{ erg cm}^{-2} \text{ s}^{-1}$ (limited to within 100 Mpc) shows ~ 30 per cent of the sources at these luminosities in the catalogue are likely background contamination, and only ~ 15 per cent of the spiral galaxy population (Sutton et al., in prep.). This is fairly similar to that found for the whole ULX luminosity range, so it seems that the fractional contamination remains roughly constant with luminosity, hence removing such sources would primarily effect the normalisation rather than the shape of the luminosity function.

The luminosity functions presented are still ultimately limited by low number statistics at the highest luminosities, which severely limits the comparison of complex models. So, although we conclude that our data do not require anything more than simple power-law models, we cannot rule out the presence of an intrinsic cut-off in the ULX luminosity function at $L_c \sim 2 \times 10^{40} \text{ erg s}^{-1}$. However, the complete sub-sample has 5 sources in its highest bin, which nominally lies above this break. If the value adopted for H_0 is significantly underestimated then source luminosities might be systematically overestimated, but this seems unlikely given the currently favoured value of $H_0 = 72 \pm 8 \text{ km s}^{-1} \text{ Mpc}^{-1}$ (Freedman et al. 2001). Given the expected level of contamination it is also unlikely these are all foreground/background sources. They must therefore be regarded as *bona fide* ULX candidates beyond the previously reported limit, which must call into question the veracity of this proposed feature. Indeed, the full catalogue contains an additional 38 sources above this proposed upper limit, although we note again that *Chandra* follow-up of all of these high luminosity sources is strictly required to confirm their nature as single point sources.

Even though these additional sources may not be included in our quantitative analysis of the luminosity function due to incompleteness, their simple presence in the catalogue carries interesting implications with respect to the possible presence of this luminosity cut-off. We first consider the case that these sources represent a smooth continuation of the universal HMXB luminosity function observed below $\sim 10^{40} \text{ erg s}^{-1}$. This luminosity is the Eddington luminosity (L_E) for a $100 M_{\odot}$ black hole, or $10 L_E$ for a $10 M_{\odot}$ black hole. One way in which higher luminosities may be explained is to invoke larger black holes. If there is no upper limit to the HMXB X-ray luminosity, then their luminosity function no longer provides evidence for an upper limit to the HMXB black hole mass. The situation is complicated by the possibility that some XRBs appear to radiate at super-Eddington rates (*e.g.* GRS 1915+105; Done et al. 2004), so an upper mass limit could still be present without manifesting itself clearly in the luminosity function. Zampieri & Roberts (2009) independently argue that even in low metallicity environments it is not possible to produce black holes significantly more massive than $\simeq 90 M_{\odot}$ through standard stellar evolution. However, a smooth luminosity function would nevertheless remove an important observational result supporting such an upper mass limit.

The lack of a high luminosity cut-off would also raise interesting questions on the nature of the relationship between the total X-ray luminosity from HMXBs in a galaxy and its star formation rate presented by Gilfanov et al. (2004a) and Gilfanov et al. (2004b). They argue that an upper limit to the HMXB luminosity function is required to produce the linear regime of their relation at high star formation rates, based on the non-trivial statistics of number distributions that follow a power-law. This linear regime requires that

the probability distribution of the total HMXB X-ray luminosity is Gaussian, which may only occur for galaxies with high enough star formation rates such that there are a fair number of sources at or near the upper limit. These sources dominate the total HMXB X-ray luminosity and remove the discrepancy between the mean and the mode values for this quantity which is otherwise present for populations drawn from luminosity functions with exponents $1 < \alpha < 2$, and causes the non-linear regime at low star formation rates. Without an upper luminosity limit, this non-linear regime should continue to higher star formation rates. However, the data do not appear to continue this trend (Gilfanov et al. 2004b), which would be an important discrepancy to address. We note briefly that the data presented in those works do not account for intrinsic absorption and obscuration, which may play an important role. Unfortunately, attempting to account for this invariably leads to model based assumptions and uncertainties.

We now also consider the case that there *is* a cut-off in the HMXB luminosity function at $\sim 2 \times 10^{40} \text{ erg s}^{-1}$. As argued previously, although it may be that the luminosities of some of the sources included in the catalogue that appear in excess of this limit have been poorly estimated, and some sources may turn out to be background quasars, this is unlikely to be the case for all 43. We would then be observing a population of sources radiating above the maximum HMXB luminosity. These must represent a different class of black hole, with a different formation mechanism. There is speculation that galaxies in the highest star formation regime may produce a population of IMBHs through black hole mergers in dense stellar clusters (see *e.g.* Gilfanov et al. 2004b; Portegies Zwart et al. 2004), which could be seen at luminosities in excess of $10^{40} \text{ erg s}^{-1}$. Fig. 10 in that work shows the effect such a population might have on the universal HMXB luminosity function; the cut-off instead becomes a step-like feature due to the upper HMXB mass limit, and above this step a far less numerous population of IMBHs are observed. Given the links between ULXs and star formation, it might not be unreasonable to argue that by focusing on galaxies that host ULXs, we are selecting galaxies with high star formation rates. The presence of such high luminosity sources in our catalogue therefore might not be surprising even in the presence of an upper limit to the HMXB black hole mass, and may be evidence for a rare population of IMBHs. These intriguing sources are investigated further in Sutton et al. (in prep.).

3.2 Specific ULX Frequency

Here we again make use of the complete sub-sample to mimic the analysis presented by Swartz et al. (2008), and investigate how the specific ULX frequency S^u , *i.e.* the number of ULXs per unit galaxy mass, evolves as a function of galaxy mass. This provides additional information on the type of galaxy, and hence the environments in which ULXs are preferentially formed. In order to estimate galaxy mass for the galaxies with complete observations, we make use of the relations between optical colour and stellar mass-to-light ratio, M/L , presented in Bell et al. (2003), which should hold for both elliptical and spiral type galaxies (we are assuming that stellar mass is directly proportional to galaxy mass). The derivation of these relations utilises SDSS data (York et al. 2000) and the PÉGASE galaxy evolution models (updated from those originally presented in Fioc & Rocca-Volmerange 1997), and assumes a scaled version of the Salpeter Initial Mass Function (the same as adopted in earlier work by Bell & de Jong 2001). We choose to calculate M/L in the B -band, and utilise the B -band magnitude and the $(B - V)$ colours provided in RC3 to estimate

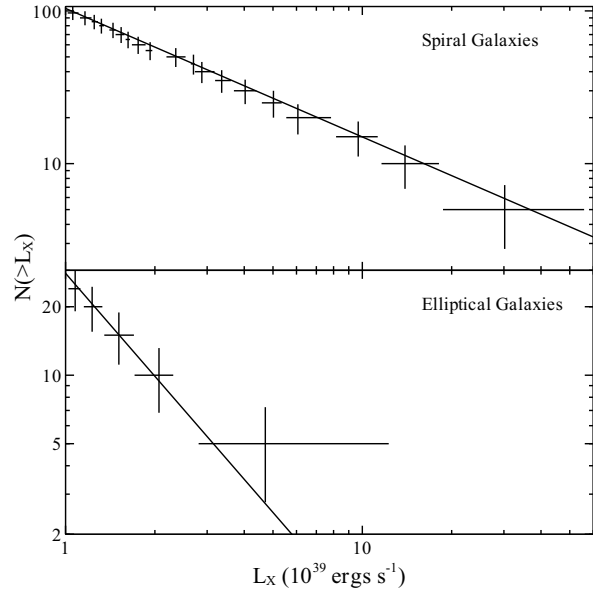


Figure 8. The luminosity functions for sources in the complete subset located in spiral galaxies (top) and elliptical galaxies (bottom). Again, the best fit power-law model to each is also shown.

the galaxy mass. The scatter around the relation between M/L_B and $(B - V)$ is estimated to be ~ 0.1 dex, so we include this in the estimated uncertainty of our M/L_B values. The colours and magnitudes used have been corrected for Galactic and internal extinction, and for redshift, and when converting absolute magnitudes to solar B -band luminosities, we adopt an absolute solar B -band magnitude of 5.47 (Cox 2000).

Through this method, stellar mass estimates were obtained for 86 and 35 of the 108 and 56 complete spiral and elliptical galaxies respectively. Galaxies without mass estimates, which were mainly a mixture of elliptical and small nearby galaxies (in particular dwarf spheroidal galaxies), were discarded from our analysis. For each galaxy with a mass estimate, we counted the number of ULX candidates assumed to be associated with it. As with the luminosity function analysis, we attempt to minimize the effects of transient and highly variable sources by considering only sources detected in the longest observation of each galaxy. Then, grouping all the complete galaxies into equally spaced decade mass bins, we calculate S^u for each bin by dividing the total number of ULX candidates observed by the total galaxy mass contained within that bin. This is expressed in equation 6 for the i th bin containing n_i galaxies:

$$S_i^u = \frac{N_i}{M_i} = \frac{\sum_{j=1}^{n_i} N_j}{\sum_{j=1}^{n_i} M_j} \quad (6)$$

where N_i and M_i are the total number of ULXs and the total galaxy mass in bin i respectively, N_j is the number of ULXs associated with the j th galaxy within that bin, and M_j is the mass of that galaxy. Fig. 9 shows the specific ULX frequency plotted as a function of galaxy mass, as well as the number of galaxies contributing to each bin, the number of ULX candidates in each bin, and the total galaxy mass in each bin.

It is clear from Fig. 9 that S^u decreases with increasing galaxy mass, qualitatively similar to the trend presented in Swartz et al. (2008) with a sample compiled from *Chandra*, *XMM-*

Newton and *ROSAT* observations of catalogued galaxies within ~ 8 Mpc (Karachentsev et al. 2004). Phenomenologically we fit the data (only for bins in which ULX candidates have been detected) with a power-law, *i.e.* $S^u \propto M^{-\beta}$ and obtain an index of $\beta = 0.59 \pm 0.07$ (1σ uncertainties). With this relation, it becomes immediately apparent why no ULX candidates are detected in the few lowest mass bins. The prediction, by extrapolation, for S^u in the highest mass bin without a detection is 7×10^{-4} ULXs per 10^6 solar masses which, considering the total stellar mass contained within that bin, equates to less than one (~ 0.4) expected ULX detection. For even lower mass bins, the estimated number of ULX detections continues to decrease; there is simply not enough galaxy mass contained in the low mass bins to expect ULXs to be detected. The lack of detections in these bins is therefore not inconsistent with the trend observed for the bins *with* ULX detections. We also calculate S^u for spiral and elliptical galaxies separately, as shown in Fig. 10, and also fit these data with power-law models. The indices obtained are $\beta_{\text{spiral}} = 0.64 \pm 0.07$ and $\beta_{\text{elliptical}} = -0.5^{+0.3}_{-0.5}$. As is clear from Fig. 10, such a model does not provide as excellent a representation of the data for elliptical galaxies as it does for spiral galaxies. However, we stress that due to a lack of ULX detections and galaxies with mass estimates, as well as the higher fractional contamination, the quality of the elliptical data is rather poor. This is reflected in the large uncertainty on the elliptical index, which is in fact consistent with zero, *i.e.* the case where S^u is constant with galaxy mass. Unsurprisingly, since the complete sample is dominated by sources associated with spiral galaxies, the results obtained for this population are very similar to the results obtained for the whole sub-sample.

Before discussing the potential physical origins of these results, it is important to consider possible biases that may be present. By considering only sources detected in the longest observation of each galaxy, we hope to have minimised the influence of transient sources as best we can. Background contaminants may have an important effect here, but as argued in Swartz et al. (2008), they are more likely to be prominent in the larger, higher mass galaxies, primarily because they cover a much greater sky area. This serves to artificially increase the number of ULX candidates and hence S^u in the higher mass bins, and to flatten the observed trend, *i.e.* decrease β . If these sources are important, the values of β presented here may only be lower limits. Other biases may arise due a combination of our ULX selection criteria and the fairly modest resolution of *XMM-Newton*. By excluding the nuclear regions of galaxies and extended sources there will be ULXs in the observed galaxies that are not included in our catalogue. Since we have defined the nuclear region with approximately a constant angular size, a greater physical area will be excluded for more distant galaxies. This is important as the radial distribution of ULX candidates peaks toward the centres of galaxies (Swartz et al. 2004; Liu et al. 2006). On average, the higher mass galaxies are further away, so this too will have a more important effect on the higher mass bins, and the number of ULXs in those bins may be slightly underpredicted. In terms of the exclusion of extended sources, of which star forming regions may contribute a large number, both galaxy star formation rate and stellar mass will determine the number of ULXs missed through being embedded within them. It is not immediately clear whether this should have any preferential effect on any region of the mass scale. Finally, there is also the possibility that some of the 2XMM detections are actually a number of unresolved point sources, but again it is not clear whether this should have a greater effect on any range of the mass scale than others. However, while these considerations may have an effect on the quantitative forms of the relations

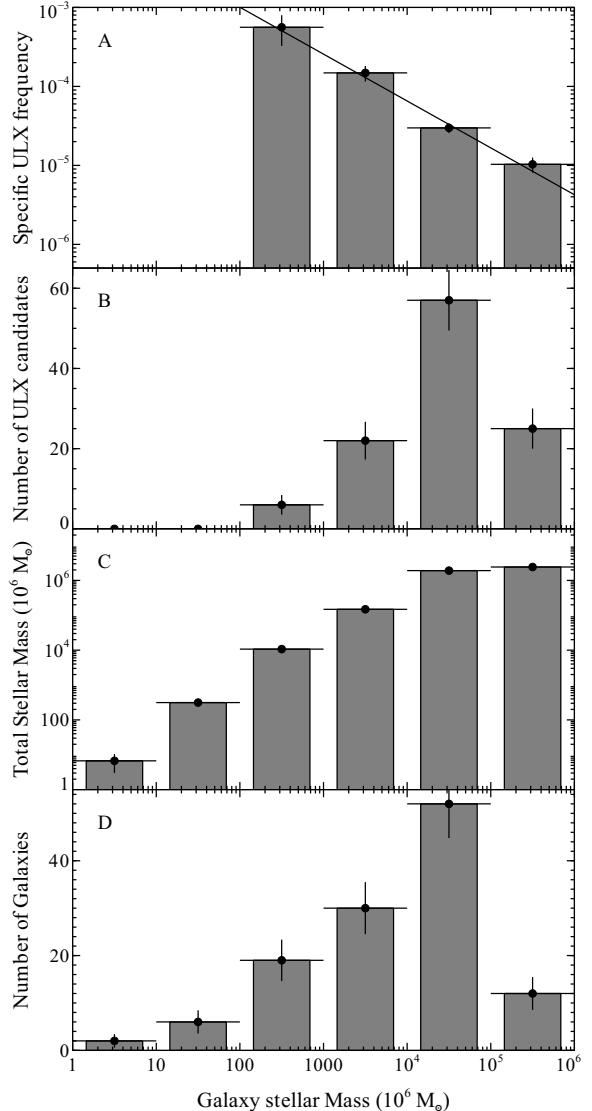


Figure 9. The specific ULX frequency and the best fit power-law model (panel A; see text), total observed ULX candidate detections (panel B), total stellar mass and number of galaxies (panels C and D) as a function of galaxy stellar mass for galaxies with complete observations included in 2XMM.

presented, given the similar trend presented by Swartz et al. (2008) to that found here for spiral galaxies, we can be confident in the qualitative form of this result.

It is clear that the number of ULXs per unit stellar mass decreases with increasing galaxy mass for spiral galaxies. There are two main physical differences between low mass and high mass spirals that are likely to be combining to give this effect. The first is that the specific star formation rate, *i.e.* the star formation rate per unit mass, is higher on average for lower mass spirals (see Fig. 24 in Brinchmann et al. 2004). ULXs are well correlated with star forming regions (Swartz et al. 2009), and there are typically a larger number of ULXs in galaxies with high star formation rates (Grimm et al. 2003). The second is that lower mass galaxies typically have lower metallicities (Lee et al. 2006). ULXs are often observed to be located in low metallicity regions (see *e.g.* Soria et al. 2005, Zampieri & Roberts 2009, Mapelli et al. 2009, Mapelli et al. 2010), and there are a number of theoretical considerations that suggest the $M_{BH} > 10 M_{\odot}$ black holes some ULXs are specu-

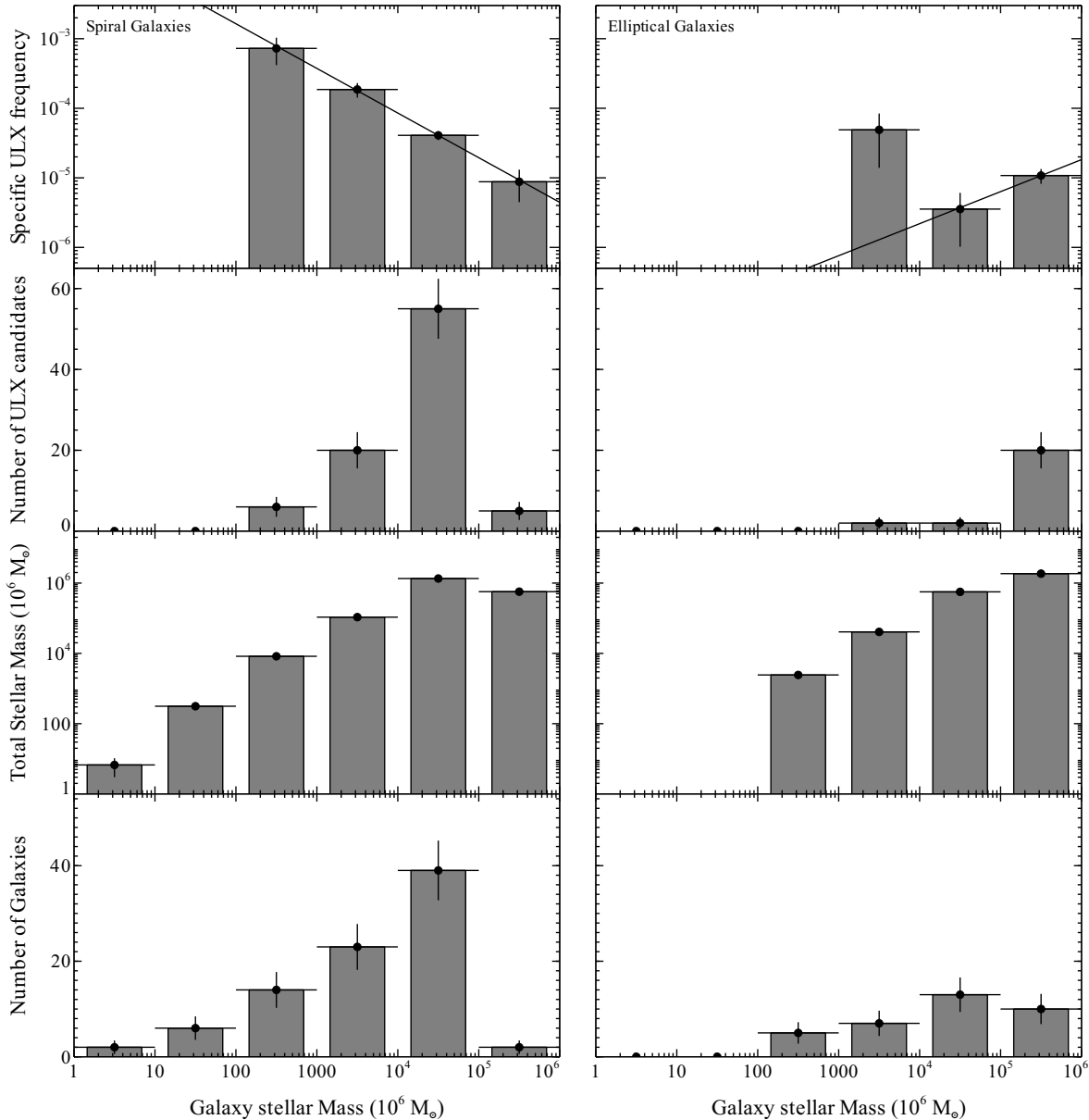


Figure 10. The specific ULX frequency and the best fit power-law model calculated for spiral (left column) and elliptical galaxies (right column) separately. The vertical panels are as in Fig. 9.

lated to host are easier to form in these regions, both due to the formation of larger progenitor stars, and reduced mass loss rates from stellar winds (Madau & Rees 2001; Bromm 2004; Vink et al. 2001; Heger et al. 2003). This combination of higher star formation per unit mass and lower metallicity provides a natural explanation for the higher specific ULX frequency in low mass spirals. However, we stress that this does not necessarily mean ULXs are commonly observed in low mass galaxies, for the same reason that there are no ULX detections in the very lowest mass bins. Although we find there are more ULXs per unit mass in lower mass spiral galaxies, a large number of these galaxies often need to be observed to detect ULXs by virtue of the fact they do not contain much mass.

Although the elliptical data is consistent with S^u remaining constant with galaxy mass, we briefly comment on the possibility that S^u might increase with increasing elliptical galaxy mass as formally suggested by the exponent obtained, as such a scenario

would be very interesting. When stellar binary systems undergo supernova, they experience a velocity kick (Harrison et al. 1993; Frail et al. 1994; Lyne & Lorimer 1994), and over the course of the lifetime of a galaxy some fraction of its binary systems may be ejected. It might be that a larger fraction of binaries are ejected from lower mass galaxies than higher mass galaxies owing to their weaker gravitational potentials. This effect might lead to such a positive trend in elliptical galaxies where ULXs are expected to be LMXBs, hence star formation and metallicity effects are likely to be minimal. However, we stress again that the data are consistent with S^u being constant with stellar mass, which would be a simpler scenario to explain given that LMXBs are expected to trace stellar mass (Gilfanov 2004).

4 CONCLUSIONS

Through cross correlation with the RC3 galaxy catalogue, we have mined the 2XMM Serendipitous Survey to produce a catalogue of ULX candidates. Our catalogue contains 650 detections of 470 discrete sources, and we conservatively estimate that at most ~ 24 per cent, but more likely ~ 17 per cent of these sources are undesirable contaminants, most likely background quasars in this case. Our catalogue offers a significant improvement in the number of ULX candidates on that of Swartz et al. (2004), which was previously the largest uniformly selected, dedicated ULX catalogue published to date. Obviously one of the key potential uses of this resource is to unearth and provide basic information on sources for which more detailed observation and/or analysis would be both interesting and insightful. One such source that we draw attention to is NGC 470 HLX1, a detailed analysis of which will be included in forthcoming work by Sutton et al. (in prep). In addition to highlighting interesting sources, the catalogue may also be used to directly analyse what we hope to be a representative sample of the whole ULX population.

To undertake statistical studies of the ULX population, we define a ‘complete’ sub-sample of the population taken only from galaxies with observations sensitive enough that we would expect all the ULX candidates in those galaxies that meet our selection criteria to be detected. The limitations of these criteria have been discussed in detail in §2.5 and are not repeated here. The luminosity function of this sample is well modelled with a single, unbroken power-law of form $N(>L_X) \propto L_X^{-0.96 \pm 0.11}$. We do not find any evidence for a break or cut-off in the luminosity function at $L_X \sim 2 \times 10^{40}$ erg s $^{-1}$, as has previously been reported in Swartz et al. (2004) and Grimm et al. (2003) and, in the latter case, interpreted as possible evidence for an upper limit of $\sim 100 M_\odot$ to HMXB black hole masses. However, given the possible biases introduced by *e.g.* non-systematic uncertainties in galaxy distances, we certainly cannot rule out the intrinsic presence of any such cut-off. Additional *Chandra* observations with increased sensitivity of a greater number of nearby galaxies would help to address this issue. Similar to results obtained in previous work, *e.g.* Swartz et al. (2004), there is also tentative evidence that the luminosity function of ULXs in elliptical galaxies is steeper than that of ULXs in spiral galaxies, which would be consistent with the assumption that elliptical galaxy ULXs are primarily low mass binary systems, while those in spiral galaxies are high mass systems.

We find that the specific ULX frequency S^u , *i.e.* the number of ULXs per unit galaxy mass, decreases with increasing galaxy mass for ULXs associated with spiral galaxies, and is well modelled with a power-law of form $S^u \propto M^{-0.64 \pm 0.07}$. Although the quantitative form of this relation may be affected by biases such as background contamination, we are confident that the qualitative trend is robust, as it is similar to the result presented in Swartz et al. (2008). This trend may be due to a combination of the increase in specific star formation rate and the decrease in metallicity with decreasing spiral galaxy mass (Brinchmann et al. 2004; Lee et al. 2006). The specific ULX frequency for elliptical galaxies is found to be consistent with being constant with galaxy mass, as expected given that LMXBs should trace stellar mass rather than star formation (Gilfanov 2004).

The population analysis presented here is by no means comprehensive, rather a number of examples of the work that is possible with the offered resource. We hope that the construction of this catalogue will encourage future authors to continue this work and so we make the catalogue available online with this publica-

tion⁹; other interesting possibilities may be to re-visit the connection between ULXs and star formation, and to search for further similarities and/or differences between ULXs in spiral and elliptical galaxies to confirm their HMXB/LMXB nature. The successes and limitations of our analysis highlight the importance of utilising both the *XMM-Newton* and *Chandra* observatories to discover and study ULXs. A number of the limitations are due to the more modest angular resolution of *XMM-Newton*. The improvement in this area offered by *Chandra* is essential to confirm the point-like nature of ULX candidates, and perhaps resolve additional sources that *XMM-Newton* could not. However, the larger effective area of *XMM-Newton* provides detections with better photon statistics, particularly at high energies, enabling analysis that would not be possible with the *Chandra* satellite, *e.g.* detecting high energy spectral curvature (Stobbart et al. 2006; Gladstone et al. 2009; Walton et al. 2011; Middleton et al. 2011; Walton et al. in prep.).

This work also highlights the importance of serendipity within astronomy. Catalogues such as 2XMM are vital resources for unearthing new examples and studying populations of various astrophysical objects. Based on the success of our compilation, we anticipate that future releases of *XMM-Newton* source catalogues, will contain many more ULXs again, providing a further significant contribution to improving our understanding of the characteristics and diversity of the ULX population.

ACKNOWLEDGEMENTS

The authors would like to thank the referee for their useful suggestions, which have helped improve this paper, and also acknowledge the financial support provided by the UK STFC research council. Some of the figures included in this work have been produced with the *Veusz*¹⁰ plotting package, written by Jeremy Sanders. This work is based on *XMM-Newton* observations, an ESA mission with instruments and contributions directly funded by ESA member states and the USA (NASA). In addition, this research has made use of the NASA/IPAC Extragalactic Database (NED), operated by the Jet Propulsion Laboratory, California Institute of Technology, as well as the Digitised Sky Survey (DSS), produced at the Space Telescope Science Institute under U.S. Government grant NAG W-2166.

REFERENCES

- Abramowicz M. A., Calvani M., Nobili L., 1980, *ApJ*, 242, 772
- Begelman M. C., King A. R., Pringle J. E., 2006, *MNRAS*, 370, 399
- Bell E. F., de Jong R. S., 2001, *ApJ*, 550, 212
- Bell E. F., McIntosh D. H., Katz N., Weinberg M. D., 2003, *ApJS*, 149, 289
- Brinchmann J., Charlot S., White S. D. M., Tremonti C., Kauffmann G., Heckman T., Brinkmann J., 2004, *MNRAS*, 351, 1151
- Bromm V., 2004, *PASP*, 116, 103
- Carrera F. J. et al., 2007, *A&A*, 469, 27
- Cash W., 1979, *ApJ*, 228, 939
- Colbert E. J. M., Heckman T. M., Ptak A. F., Strickland D. K., Weaver K. A., 2004, *ApJ*, 602, 231

⁹ Catalogue to be made available online via MNRAS; available in the meantime via private communication

¹⁰ <http://home.gna.org/veusz/>

- Colbert E. J. M., Mushotzky R. F., 1999, *ApJ*, 519, 89
- Colbert E. J. M., Ptak A. F., 2002, *ApJS*, 143, 25
- Cox A. N., 2000, *Allen's Astrophysical Quantities* (4th ed.; New York: Springer)
- Davis D. S., Mushotzky R. F., 2004, *ApJ*, 604, 653
- de Vaucouleurs G., de Vaucouleurs A., Corwin H. G., Jr., Buta R. J., Paturel G., Fouque P., 1991, *The Third Reference Catalogue of Bright Galaxies* (New York: Springer)
- Done C., Wardziński G., Gierliński M., 2004, *MNRAS*, 349, 393
- Fabbiano G., 1989, *ARA&A*, 27, 87
- Farrell S. A., Webb N. A., Barret D., Godet O., Rodrigues J. M., 2009, *Nat*, 460, 73
- Finke J. D., Böttcher M., 2007, *ApJ*, 667, 395
- Fioc M., Rocca-Volmerange B., 1997, *A&A*, 326, 950
- Frail D. A., Goss W. M., Whiteoak J. B. Z., 1994, *ApJ*, 437, 781
- Freedman W. L. et al., 2001, *ApJ*, 553, 47
- Gao Y., Wang Q. D., Appleton P. N., Lucas R. A., 2003, *ApJ*, 596, L171
- Ghosh H., Mathur S., Fiore F., Ferrarese L., 2008, *ApJ*, 687, 216
- Gilfanov M., 2004, *MNRAS*, 349, 146
- Gilfanov M., Grimm H., Sunyaev R., 2004a, *MNRAS*, 347, L57
- Gilfanov M., Grimm H., Sunyaev R., 2004b, *MNRAS*, 351, 1365
- Gladstone J. C., Roberts T. P., Done C., 2009, *MNRAS*, 397, 1836
- Grimm H., Gilfanov M., Sunyaev R., 2003, *MNRAS*, 339, 793
- Harrison P. A., Lyne A. G., Anderson B., 1993, *MNRAS*, 261, 113
- Hasinger G., 2004, *Nuclear Physics B Proceedings Supplements*, 132, 86
- Heger A., Fryer C. L., Woosley S. E., Langer N., Hartmann D. H., 2003, *ApJ*, 591, 288
- Humphrey P. J., Fabbiano G., Elvis M., Church M. J., Bałucińska-Church M., 2003, *MNRAS*, 344, 134
- Jenkins L. P., Roberts T. P., Ward M. J., Zezas A., 2004, *MNRAS*, 352, 1335
- Jonker P. G., Torres M. A. P., Fabian A. C., Heida M., Miniutti G., Pooley D., 2010, *MNRAS*, 407, 645
- Kaaret P., Ward M. J., Zezas A., 2004, *MNRAS*, 351, L83
- Kalberla P. M. W., Burton W. B., Hartmann D., Arnal E. M., Bajaja E., Morras R., Pöppel W. G. L., 2005, *A&A*, 440, 775
- Karachentsev I. D., Karachentseva V. E., Huchtmeier W. K., Makarov D. I., 2004, *AJ*, 127, 2031
- King A. R., 2002, *MNRAS*, 335, L13
- King A. R., 2008, *MNRAS*, 385, L113
- King A. R., Davies M. B., Ward M. J., Fabbiano G., Elvis M., 2001, *ApJ*, 552, L109
- Lee H., Skillman E. D., Cannon J. M., Jackson D. C., Gehrz R. D., Polomski E. F., Woodward C. E., 2006, *ApJ*, 647, 970
- Lehmer B. D., Alexander D. M., Bauer F. E., Brandt W. N., Goulding A. D., Jenkins L. P., Ptak A., Roberts T. P., 2010, *ApJ*, 724, 559
- Lira P., Ward M., Zezas A., Alonso-Herrero A., Ueno S., 2002, *MNRAS*, 330, 259
- Liu J., 2011, *ApJS*, 192, 10
- Liu J., Bregman J. N., 2005, *ApJS*, 157, 59
- Liu J., Bregman J. N., Irwin J., 2006, *ApJ*, 642, 171
- Liu Q. Z., Mirabel I. F., 2005, *A&A*, 429, 1125
- Lyne A. G., Lorimer D. R., 1994, *Nat*, 369, 127
- Madau P., Rees M. J., 2001, *ApJ*, 551, L27
- Mapelli M., Colpi M., Zampieri L., 2009, *MNRAS*, 395, L71
- Mapelli M., Ripamonti E., Zampieri L., Colpi M., Bressan A., 2010, *MNRAS*, 408, 234
- Mateos S. et al., 2008, *A&A*, 492, 51
- Middleton M. J., Roberts T. P., Done C., Jackson F. E., 2011, *MNRAS*, 411, 644
- Miller M. C., Colbert E. J. M., 2004, *International Journal of Modern Physics D*, 13, 1
- Moretti A., Campana S., Lazzati D., Tagliaferri G., 2003, *ApJ*, 588, 696
- Pakull M. W., Grisé F., 2008, in *American Institute of Physics Conference Series*, Vol. 1010, R. M. Bandyopadhyay, S. Wachter, D. Gelino, & C. R. Gelino, ed, *A Population Explosion: The Nature & Evolution of X-ray Binaries in Diverse Environments*, p. 303
- Pakull M. W., Mirioni L., 2003, in *Revista Mexicana de Astronomia y Astrofisica*, vol. 27, Vol. 15, J. Arthur & W. J. Henney, ed, *Revista Mexicana de Astronomia y Astrofisica Conference Series*, p. 197
- Piconcelli E., Cappi M., Bassani L., Di Cocco G., Dadina M., 2003, *A&A*, 412, 689
- Portegies Zwart S. F., Baumgardt H., Hut P., Makino J., McMillan S. L. W., 2004, *Nat*, 428, 724
- Poutanen J., Lipunova G., Fabrika S., Butkevich A. G., Abolmasov P., 2007, *MNRAS*, 377, 1187
- Rappaport S. A., Podsiadlowski P., Pfahl E., 2005, *MNRAS*, 356, 401
- Remillard R. A., McClintock J. E., 2006, *ARA&A*, 44, 49
- Reynolds C. S., Loan A. J., Fabian A. C., Makishima K., Brandt W. N., Mizuno T., 1997, *MNRAS*, 286, 349
- Roberts T. P., 2007, *Astrophysics and Space Science*, 311, 203
- Soria R., Cropper M., Pakull M., Mushotzky R., Wu K., 2005, *MNRAS*, 356, 12
- Stobbart A.-M., Roberts T. P., Wilms J., 2006, *MNRAS*, 368, 397
- Sutton A. D., Roberts T. P., Walton D. J., 2010, *ArXiv e-prints*
- Swartz D. A., Ghosh K. K., Tennant A. F., Wu K., 2004, *ApJS*, 154, 519
- Swartz D. A., Soria R., Tennant A. F., 2008, *ApJ*, 684, 282
- Swartz D. A., Tennant A. F., Soria R., 2009, *ApJ*, 703, 159
- Tully R. B., 1988, *Nearby Galaxies Catalog* (Cambridge: Cambridge University Press)
- Vink J. S., de Koter A., Lamers H. J. G. L. M., 2001, *A&A*, 369, 574
- Walton D. J., Gladstone J. C., Roberts T. P., Fabian A. C., Caballero-Garcia M. D., Done C., Middleton M. J., 2011, *MNRAS*, 684
- Watson M. G. et al., 2009, *A&A*, 493, 339
- Wong D. S., Chornock R., Filippenko A. V., 2008, *PASP*, 120, 266
- York D. G. et al., 2000, *AJ*, 120, 1579
- Zampieri L., Roberts T. P., 2009, *MNRAS*, 400, 677
- Zezas A., Fabbiano G., Baldi A., Schweizer F., King A. R., Rots A. H., Ponman T. J., 2007, *ApJ*, 661, 135
- Zhang W. M., Soria R., Zhang S. N., Swartz D. A., Liu J. F., 2009, *ApJ*, 699, 281

APPENDIX A: EXAMPLE CATALOGUE ENTRIES**Table A1.** Some basic information for example entries in the presented catalogue, including the PGC galaxy identifier, the adopted galaxy distance, the 2XMM source ID, the detection luminosity, potential matches in previous catalogues (Colbert & Ptak 2002: CP02; Liu & Bregman 2005: LB05; Swartz et al. 2004: SW04; Liu & Mirabel 2005: LM05) and flags detailing whether the source is a ‘new’ ULX candidate (*i.e.* not present in any of the above catalogues) and whether the source detection is included in the complete subset.

PGC	Distance (Mpc)	2XMM Source ID	Detection Luminosity (10^{39} erg s $^{-1}$)	CP02 Name	LB05 Name	SW04 RecNo	LM05 Name	New?	Complete Subset?
1370	45.77	2609	2.25 ± 0.77					yes	no
1388	45.0	2677	3.27 ± 0.80					yes	no
2248	120.96	4975	5.12 ± 2.18					yes	no
2388	58.21	5291	2.50 ± 0.76					yes	no
2789	3.0	7278	1.35 ± 0.01					yes	yes
2789	3.0	7278	1.18 ± 0.02					yes	yes
2789	3.0	7278	0.38 ± 0.01					yes	yes
2789	3.0	7278	0.87 ± 0.05					yes	yes
2789	3.0	7337	1.62 ± 0.02				NGC 253 ULX2	no	yes
2789	3.0	7337	1.63 ± 0.02				NGC 253 ULX2	no	yes
2789	3.0	7337	2.26 ± 0.04				NGC 253 ULX2	no	yes
2789	3.0	7337	2.47 ± 0.06				NGC 253 ULX2	no	yes
3453	75.29	9158	14.38 ± 2.65					yes	no
4777	34.12	12122	153.03 ± 7.98					yes	no
4801	30.87	12156	1.83 ± 1.09					yes	no
5098	65.65	12557	14.16 ± 4.07					yes	no
5193	27.45	12818	1.42 ± 0.70					yes	no
5193	27.45	12821	0.99 ± 0.63					yes	no
5283	73.84	13038	10.74 ± 2.40					yes	no
5283	73.84	13038	17.58 ± 9.63					yes	no
5974	9.70	14174	2.73 ± 0.15				NGC 628 ULX2	no	yes
5974	9.70	14223	1.91 ± 0.17				NGC 628 ULX1	no	yes
5974	9.70	14223	1.04 ± 0.15				NGC 628 ULX1	no	yes
6983	22.88	15962	1.57 ± 0.32			5	NGC 720 ULX7/8	no	no
6983	22.88	15962	1.69 ± 0.77			5	NGC 720 ULX7/8	no	no
7252	74.15	16228	11.10 ± 3.64					yes	no
7584	66.47	16743	13.24 ± 6.90					yes	no
8726	71.21	18486	1.78 ± 1.59					yes	no
8974	31.25	20178	17.66 ± 5.73					yes	no
9067	83.01	21018	23.64 ± 3.71					yes	no
9578	68.36	23745	16.04 ± 15.78					yes	no
10122	18.76	25071	0.78 ± 0.29					yes	no
10122	18.76	25091	50.51 ± 2.15	IXO 4	NGC 1042 ULX1		NGC 1042 ULX1	no	no
10122	18.76	25091	29.54 ± 2.40	IXO 4	NGC 1042 ULX1		NGC 1042 ULX1	no	no
10175	19.65	25272	0.90 ± 0.20					yes	yes
10175	19.65	25272	0.73 ± 0.26					yes	no
10266	14.57	25719	1.08 ± 0.07					yes	yes
10266	14.57	25703	0.91 ± 0.12		NGC 1068 ULX2			no	yes
10266	14.57	25703	0.86 ± 0.13		NGC 1068 ULX2			no	yes
10314	9.1	25840	1.02 ± 0.13				NGC 1058 ULX1	no	yes
10959	69.36	26594	34.03 ± 7.33					yes	no
12209	8.6	28959	2.81 ± 0.11	IXO 6	NGC 1291 ULX1	12	NGC 1291 ULX3	no	yes
12286	3.70	29101	1.08 ± 0.06					yes	yes
12286	3.70	29250	5.84 ± 0.06	IXO 7	NGC 1313 ULX1		NGC 1313 ULX1	no	yes
12286	3.70	29250	11.52 ± 0.15	IXO 7	NGC 1313 ULX1		NGC 1313 ULX1	no	yes
12286	3.70	29250	8.89 ± 0.16	IXO 7	NGC 1313 ULX1		NGC 1313 ULX1	no	yes
12286	3.70	29250	6.61 ± 0.13	IXO 7	NGC 1313 ULX1		NGC 1313 ULX1	no	yes
12286	3.70	29250	7.14 ± 0.14	IXO 7	NGC 1313 ULX1		NGC 1313 ULX1	no	yes
12286	3.70	29250	11.03 ± 0.21	IXO 7	NGC 1313 ULX1		NGC 1313 ULX1	no	yes
12286	3.70	29250	8.88 ± 0.19	IXO 7	NGC 1313 ULX1		NGC 1313 ULX1	no	yes
12286	3.70	29250	7.98 ± 0.23	IXO 7	NGC 1313 ULX1		NGC 1313 ULX1	no	yes
12286	3.70	29250	10.71 ± 0.29	IXO 7	NGC 1313 ULX1		NGC 1313 ULX1	no	yes
12286	3.70	29250	7.71 ± 0.28	IXO 7	NGC 1313 ULX1		NGC 1313 ULX1	no	yes
12286	3.70	29250	9.10 ± 0.43	IXO 7	NGC 1313 ULX1		NGC 1313 ULX1	no	yes
12286	3.70	29250	3.23 ± 0.06	IXO 7	NGC 1313 ULX1		NGC 1313 ULX1	no	yes